IPNO-DRE 95-08

THE LOW-SPIN STATES IN THE DOUBLY-ODD ^{182}Ir NUCLEUS AND THE INFLUENCE OF THE PROTON-NEUTRON INTERACTION

J. Sauvage, D. Hojman [1)], F. Ibrahim, B. Roussière,
P. Kilcher, F. Le Blanc, J. Oms,
Institut de Physique Nucléaire, 91406 Orsay Cedex, France
J. Libert
Centre d'Etudes Nucléaires de Bordeaux Gradignan
Le Haut Vigneau - 33170 Gradignan, France
and the ISOCELE Collaboration

Submitted to Nuclear Physics

THE LOW-SPIN STATES IN THE DOUBLY-ODD ^{182}Ir NUCLEUS AND THE INFLUENCE OF THE PROTON-NEUTRON INTERACTION

J. Sauvage, D. Hojman [1)], F. Ibrahim, B. Roussière, P. Kilcher, F. Le Blanc, J. Oms,
Institut de Physique Nucléaire
91406 Orsay Cedex, France

J. Libert
Centre d'Etudes Nucléaires de Bordeaux Gradignan
Le Haut Vigneau - 33170 Gradignan, France

and the ISOCELE Collaboration

1) Permanent address : Departamento de Física, CNEA, Buenos Aires, ARGENTINA

Abstract : Low-spin states of ^{182}Ir populated through the β^+/EC decay of ^{182}Pt were studied using the ISOCELE facility. A low-spin level scheme has been established. Using a semi-microscopic rotor-plus-two-quasiparticle model developed in the context of the HF + BCS approximation the influence of the $V_{p\text{-}n}$ interaction on the relative energy location of excited states has been studied and the low-spin states located at low energy in ^{182}Ir have been identified. The α-decay energy of ^{186}Au has been corrected to 4907 ± 16 keV.

Radioactivity ^{182}Pt [from Pt(p, xn)Au, on-line mass separation]; measured $E\gamma$, $I\gamma$, $\gamma\gamma t$-, (X-ray)γt-coin. ^{182}Ir deduced levels, J, π, γ-multipolarity. Hyperpure Ge.

1. INTRODUCTION

The neutron-deficient ^{184}Au and ^{182}Ir isotones are of peculiar interest because they are situated on the prolate edge of a region where shape coexistence phenomena and related ground-state shape transitions have currently been observed. Coexistences of prolate and oblate (or triaxial) shapes at normal deformation have, indeed, been established in the odd-A ^{185}Hg [refs.[1-4])] and ^{183,185}Au [refs.[2,5-9])] nuclei, neighbours of the doubly-odd ^{184}Au whereas all the single-particle states observed in the odd-A ^{183}Pt[refs.[10-12])], ^{181,183}Ir [refs.[13-22])] and ^{181}Os [refs.[23-27])] nuclei, neighbours of ^{182}Ir clearly indicate a prolate nuclear shape. Therefore an axial-rotor-plus-two-quasiparticle model is expected to well describe the doubly-odd ^{182}Ir and thus, to provide first information on the influence of the V_{p-n} interaction on nuclear properties.

In-beam experiments have recently been performed on ^{182}Ir by another group [19,28]). The observed collective structures indicate that low-energy states in the ^{182}Ir isotope actually correspond to a prolate nuclear shape on the basis of a classification scheme established for the different couplings of a proton and a neutron to each other and to a deformed core [29,30]). On the other hand, nothing was known about the low-energy and low-spin states that can be populated by radioactive decay. Therefore we have studied the low-spin states of ^{182}Ir from the β^+/EC decay of ^{182}Pt nuclei using the ISOCELE facility[31,32]).

In such a transitional doubly-odd nucleus the Coriolis force plays an important role making the analysis particularly complex. A semi-microscopic rotor-plus-two-quasiparticle model has been developed in the context of the Hartree-Fock-plus-BCS approximation[33]). This model takes into account the geometrical coupling of the proton with the neutron as well as that of each quasiparticle with the core. It consistently treats the residual V_{p-n} term using the same effective nucleon-nucleon interaction as that used in the Hartree-Fock-plus-BCS mean-field calculation and has, in principle, no adjustable parameters. In this approach axial symmetry is assumed, which is justified in this mass region for prolate-shaped states.The rotor-plus-one-quasiparticle model [34]) developed in the same context has been shown to have a predictive power for the transitional prolate-shaped odd-A nuclei[35]). Bennour[36]) has shown that similar features can be expected with the rotor-plus-two-quasiparticle approach applied in the present study. Using the predictions of this model and the results previously obtained on collective structures[19]) we will discuss the influence of the residual V_{p-n} interaction and identify the low-energy excited levels in ^{182}Ir.

2. EXPERIMENTAL PROCEDURE

Excited levels of ^{182}Ir have been populated by β^+/EC decay of ^{182}Pt ($T_{1/2}$ = 2.2 m) nuclei themselves obtained by β^+/EC decay of ^{182}Au nuclei ($T_{1/2}$ = 21 s). Gold isotopes were produced through Pt (p, xn)Au reactions ; a 7 gram Pt-B alloy target [31]) was placed inside the ion source of the ISOCELE separator[32]) and bombarded with the 200 MeV proton beam delivered by the Orsay synchrocyclotron. The ^{182}Au ions extracted from the ion source using a 30 kV high voltage were collected during 200 seconds on a mylar-aluminum tape and, after a 100 second waiting time, the obtained radioactive source was moved in front of the detector set up and counted for 300 seconds. This time cycle, favouring the Pt $\rightarrow$ Ir decay, was repeated for 24 hours. Around 4 x 10^5 ^{182}Au atoms/s were produced using a 1.2 μA proton beam intensity .

The counting set up consisted of three detectors placed at 35 mm from the radioactive sources. A planar Ge (HP) X-ray detector with a 0.6 keV FWHM resolution at 122 keV covered an energy range from 12 keV to 760 keV. Two coaxial Ge(HP) detectors with 18 % efficiency and 2.0 keV FWHM resolution at 1.33 MeV covered energy ranges from 14 keV to 1.3 MeV for one and from 40 keV to 2.7 MeV for the other one. Singles γ-spectra from the three detectors were constituted by Direct Memory Increment in a Multispectral NUMELEC [ref.[37])] while three types of coincident events were simultaneously recorded in event-by-event mode on magnetic tape of an embedded system. The data acquisition management was ensured by an embedded fast microprocessor working in CAMAC [ref.[37])].

Singles γ-spectra were analysed using the GAMANAM curve-fitting code[38]), a modified version of the GAMANAL code[39]). Energies of γ-rays belonging to the ^{182}Pt β^+/EC decay were determined using as calibration the energies of the ^{182}Ir-decay γ-lines which are also present in the spectra. The X-γ-t and γ-γ-t coincidence events were arranged to get prompt- and delayed-coincidence bidimensional matrices. These matrices were analysed using either SUN or MILFEUIL programs[40]). Examples of coincidence spectra obtained for gates on γ-lines in either the γ-γ-t matrix or the X-γ-t matrices are displayed in figs. 1-4.

3. EXPERIMENTAL RESULTS

The energies and intensities of the γ-lines belonging to the ^{182}Pt $\rightarrow$ ^{182}Ir decay are respectively listed in columns 1 and 2 of table 1. Weak-intensity γ-rays ($I_\gamma \leq 5$) that were only observed coincident with Ir X-rays are not reported in the table, their total intensity represents 2.1 % of the total intensity listed. In columns 3 and 4 are respectively indicated the main coincident γ-rays and the location in the level scheme shown in fig. 5.

The low-energy level scheme (E < 300 keV) is formed by two independant parts : the first one A shown on the left-hand side and the second one B on the right-hand side of fig. 5. A third part C has been drawn in the middle of fig. 5. It consists of four states, located at 320.7, 341.2, 381.7 and 1002 keV, which de-excite to levels of both parts A and B, and of levels that decay to three of these four states and to levels of either part A or B. The energy location of part B relatively to part A has been established through the 286.7, 306.7 and 109.9, 146.2, 168.3 keV γ-lines observed in coincidence with the 70.4 and 681.5 keV γ-rays (see fig.1 and table 1) which populate respectively the 381.7 and 320.7 keV states of part C. Thus the first level of part B is at 25.7 keV above the ground state. The existence of a level located at 8.1 keV is suggested by the observation of the 70.4 and 572.2 keV γ-rays in coincidence with the 373.6 keV γ-line (Table 1). The prompt and delayed coincident spectra for gates on the 81.5 keV γ-line as a stop signal are displayed in fig. 2. We can see that the 146.2 keV mainly appears in the delayed spectrum while the 45.4 keV appears in the prompt spectrum. Moreover the 22.2 and 24.7 keV γ-lines are in prompt coincidence with the 146.2 keV γ-ray whereas the 81.5 and 152.4 keV are in delayed coincidence. Furthermore, the sum of the 24.7 and 146.2 keV energies is equal to 170.9 keV, which suggests that the 24.7-146.2 keV cascade could be located in parallel with the 170.9 keV γ-ray. This order is confirmed by the γ-lines coincident with the 656.7 keV γ-ray in comparison with those coincident with the 681.5 keV γ-ray (fig. 1). The 170.9 γ-line is indeed observed in coincidence with the 656.7 keV while it is not observed with the 681.5 keV γ-ray. Thus the 24.7 keV transition is obviously situated above the 146.2 keV transition whereas the 22.2 keV is under the 146.2 keV transition. Furthermore, the delay mentioned above is due to a half-life that may clearly be attributed to the 152.5 keV level. The low-energy 12.6, 64.9 and 17.6 keV transitions drawn in dashed line in parts A and B of the level scheme have been observed neither in singles nor in coincident spectra but their existence is implied by coincidence relationships. Thus, the 12.6 keV transition very likely links the 87.4 and 74.8 keV levels since the main γ-rays coincident with the 87.4 keV γ-line are also coincident with the 74.8 keV one (see gate on 106.8 keV in fig. 3). Its total intensity can be estimated to be around 150 ± 30. The existence of a 64.9 keV transition connecting the 152.3 and 87.4 keV levels is deduced from the observation of the 87.4 keV in coincidence with the 58.7 keV γ-line (fig. 4). In the same way, the 261.7 and 572.2 keV γ-lines are present in the coincident spectra obtained by a gate set on the 101.5 keV γ-ray, which implies the existence of a 17.6 keV transition located either above or under the 261.7 keV one. This 17.6 keV transition has been located under the 261.7 keV transition because of the γ-lines which are observed in coincidence with the 101.5 keV γ-ray and that can then connect directly or not the 1002 and 1024.3 keV levels to the 190.2 keV state. The 172.6 keV level is drawn in dashed-line since the relative position of the 17.6 and 101.5 keV transitions could not be determined. It is worth noting that two states have almost the same energy : the first one at 152.3 keV in part A and the second at 152.5 keV in part B of the level scheme. The 77.5 and 74.8 keV γ-lines are coincident with the 58.7 keV γ-ray and their intensities in the prompt coincident

spectrum are not attenuated, which proves that the 152.3 keV level has no long half-life contrary to the 152.5 keV state (fig. 4). This allowed us to establish the existence of these two distinct states. A 69.4 keV γ- line has been observed in prompt coincidence with the 57.4, 286.7 and 70.4 keV γ-rays (figs. 3, 4). This led us to locate it between the 95.1 and 25.7 keV levels of part B of the level scheme (fig. 5). Finally, a delayed coincidence has also been observed between the 45.4 and 81.5 keV γ-rays, which involves a long half-life for the 71.1 keV state of part B.

Since most of the observed γ-rays (corresponding to 95 % of the γ intensity) have been located in the level scheme we could perform intensity balances of each level assuming E1, M1, E2 or M2 possible multipolarities for each transition. From these balances we could restrict the possible multipolarities for some of the transitions and attribute an E1 multipolarity to the 81.5 keV transition. Moreover, multipolarity of the 45.4, 74.8 and 77.5 keV transitions could be deduced from the γ-line intensities determined in coincident spectra. The results together with the methods used are summarized in table 2. The M1 and not E1 multipolarities of the 45.4 and 69.4 keV transitions respectively indicate that the 25.7, 71.1 and 95.1 keV levels have the same parity whereas the E1 multipolarity of the 81.5 keV transition implies the other parity for the 152.5 keV state. This parity change between the states connected by the 57.4 keV transition has been used to attribute an E1 multipolarity to this transition (table 2).

Using total intensities of the transitions populating the 25.7, 8.1 keV and ground states, the total disintegration intensity of ^{182}Pt was estimated to be equal to 5300 ± 750 for the gamma intensity of the 123.4 keV transition taken as $I_\gamma = 100$. Since most of the transition multipolarities are unknown, only the feeding of the levels placed above 800 keV could be validly evaluated using the estimated disintegration intensity. Using the decay energy $Q_{EC} = 2.85 \pm 0.14$ MeV reported in the mass table[41]) and the logft tables[42]) $5.8 < \log f_0 t < 6.0$, $6.9 < \log f_1 t < 7.1$ values were obtained for the 1002 keV level and $6.3 < \log f_0 t < 6.5$, $7.3 < \log f_1 t < 7.5$ for the 1024.3 keV state. Thus, from the Raman-Gove rules[43]), the β decays to these two levels correspond to allowed or first-forbidden non-unique transitions. Therefore spin and parity values $I^\pi = 0^-$, 1^- or 1^+ may be assigned to the 1002 and 1024.3 keV states.

Finally, we have to note that around 20 % of the total disintegration intensity populate the 25.7 keV state of part B but no γ-ray de-exciting this state was observed, which means that either the 25.7 keV level is an isomeric state or the decaying transition is highly converted and consequently has, at least, an E2 multipolarity.

4. DISCUSSION

In a first step, to identify the low-spin states observed in ^{182}Ir, we have used the zero-order level scheme deduced from the single-particle states observed at low energy in the neighbouring odd-A nuclei together with the ^{182}Ir results from in-beam measurements[19,28]. In what follows single-particle states will be labelled, as usual, by the main component I^{π} [$Nn_z\Lambda$] of their wave functions in the asymptotic basis except in case of decoupled states for which the spherical basis is more convenient.

4.1. Zero-order level scheme

In the odd-proton ^{183}Ir and ^{181}Ir nuclei, the ground states and the first excited levels at 15.8 keV in ^{183}Ir and 24.9 keV in ^{181}Ir were respectively identified as the 5/2$^-$ and 9/2$^-$ states of the h9/2 subshell from decay studies[13-15,20]. Numerous in-beam and decay measurements performed on ^{183}Ir [refs.[17-19]] and on ^{181}Ir [refs.[16,19-22]] have subsequently confirmed this identification. The 1/2$^+$[400] states could be located at 379.2 keV in ^{183}Ir [refs.[13,14]] and at 342.4 keV in ^{181}Ir[refs.[14,20]] from decay studies. The 9/2$^-$[514] proton state was observed at 645.5 keV in ^{183}Ir from both decay and in-beam experiments[13,14,19]. In ^{181}Ir, in-beam results suggested the level located at 366 keV[ref.[19]] as the 9/2$^-$[514] state, this assignment was recently confirmed in refs.[21,22]. On the other hand, the energy location of the 3/2$^+$[402] and 5/2$^+$[402] states in light Ir isotopes is still a debated question. The 307.0 keV level in ^{183}Ir was identified as 3/2$^+$[402] from decay study[14] and as 5/2$^+$[402] from in-beam study[18]. These different interpretations have been discussed in detail by different groups and the 307.0 keV level is most likely the 3/2$^+$ [402] state[19-21]. In ^{181}Ir, the 289.4 keV level has been associated to the 3/2$^+$[402] state from decay studies[14,20] whereas in-beam measurements suggested to associate it to the 5/2$^+$[402] state[21,22]. The half-life of the 289.5 keV level, $T_{1/2}$ = 330ns [ref.[22]] and $T_{1/2}$ = 430ns [ref.[21]], determined from in-beam experiments leads, indeed, to a hindrance factor relative to the Weisskopf estimate Fw ~ 4 x 10^7 for the 289.5 keV E1 transition similar to that of the 5/2$^+$[402] $\rightarrow$ 5/2 1/2$^-$[541] E1 transition in ^{179}Re. From the data used in ref.[20] a half-life of 430ns or 330ns for the 289.4 keV level cannot be completely ruled out. So, in the present work, we have associated the 5/2$^+$[402] state to the 289.4 keV level in ^{181}Ir according to in-beam results (for instance Fw value, g_k value and feeding intensity) that are rather convincing[21,22]. All single-particle levels observed below 600 keV in ^{181,183}Ir together with their most probable identification are shown on the left-hand side of fig. 6.

Single-particle states observed in the ^{181}Os and ^{183}Pt odd-neutron nuclei have clearly been identified from both decay and in-beam experiments. In ^{183}Pt, decay measurements allowed the identification of the single-neutron states reported on the right-hand side of fig. 6 [ref.[11]]. Moreover the rotational bands observed in in-beam experiments have properties which indicate

that they are built on the $9/2^+[624]$, $7/2^-[514]$ and $1/2^-[521]$ states[12]). This confirmed the previous identification of these three neutron states. The presence of the $1/2^-[521]$, $7/2^-[514]$ and $9/2^+[624]$ states at low energy in ^{181}Os was known through decay[24]) and in-beam[23,25,26]) studies. The $7/2^-[514]$ and $9/2^+[624]$ states were very recently located at respectively 48.9 and 156.5 keV above the $1/2^-[521]$ ground state[27]). Furthermore in this latter work the levels observed at 340.5, 367.7 and 423.6 keV could be identified as the $7/2^+[633]$, $5/2^-[512]$ and $7/2^-[503]$ states respectively. The single-particle states observed below 600 keV in ^{181}Os are also shown in fig. 6.

The zero-order level scheme of ^{182}Ir is drawn in the middle of fig. 6. It has been built by coupling the proton states present in ^{181,183}Ir to the neutron states observed in ^{181}Os and ^{183}Pt through the usual procedure[29]), the proton (neutron) energy used in ^{182}Ir is obtained by linear interpolation of the energies observed in ^{181,183}Ir (^{181}Os and ^{183}Pt) and no proton-neutron residual interaction is included. We can see in fig. 6 that the states corresponding to the $\pi h_{9/2} \otimes \nu 1/2^-[521]$, $\pi h_{9/2} \otimes \nu 7/2^-[514]$, and $\pi h_{9/2} \otimes \nu 9/2^+[624]$ are expected to be located at the lowest energies. However we have to keep in mind that this zero-order level scheme can only provide a qualitative idea of the relative energy location of the different configurations.

4.2. Identification from experimental results

The in-beam study previously performed on ^{182}Ir allowed Kreiner et al.[19]) to identify three rotational bands. A doubly-decoupled band built on the level observed at the lowest energy is associated to the $\pi h_{9/2} \otimes \nu 1/2^-[521]$ configuration. Spin and parity values $I^\pi = 5^+$ are assigned to its observed bandhead from the known properties of doubly-decoupled bands[19,44,45]). The 3^+ state corresponding to this $\pi h_{9/2} \otimes \nu 1/2^-[521]$ structure is expected to be located below and very close to the 5^+ [refs.[44,46])]. Therefore it could not be observed in the in-beam work. The above mentioned 5^+ state corresponds to the 25.7 keV level in the present decay work and the ground state very likely is the 3^+ state of the same configuration. Thus, the 25.7 keV transition $5^+ \rightarrow 3^+$ would have an E2 multipolarity, its very high conversion coefficient would explain then why the 25.7 keV γ-line was not observed in the present study. The second rotational band established in the in-beam experiment is of a compressed type[30]) and the authors[19]) propose two alternative interpretations. This band could be built on a 5^+ level lying 45.4 keV above the previously discussed 5^+ observed bandhead and, in this case, would correspond to the $\pi h_{9/2} \otimes \nu 7/2^-[514]$ configuration[19]). It could also be built on a 6^+ level lying at 39 keV above the previous one and would then correspond to the $\pi\ 5/2^+[402] \otimes \nu i_{13/2}$ configuration[19]). We can note that the first possibility is in better agreement with the zero-order level-scheme prediction (fig. 6). In any case the 5^+ level, corresponding to the $\pi h_{9/2} \otimes \nu 7/2^-[514]$ configuration is the only one observed in the decay work. It decays by the 45.4 keV transition and obsviously corresponds to the 71.1 keV level of fig. 5. This latter level has, thus, spin and parity values unambiguously determined $I^\pi = 5^+$. The third and last rotational band observed in the in-beam study has negative parity and is of

a semi-decoupled type[29,30]) It is associated to the $\pi h_{9/2} \otimes \nu i_{13/2}$ configuration and its bandhead is the initial state of the 81.5 keV E1 transition[19]). The bandhead of this structure is the 152.5 keV level established in the present work. This level was first proposed as the (5^-) member[19]) and very recently as the (4^-) member[28]) of this configuration. Furthermore, in the latter work the (6^-) member is at 24 keV above the (4^-) state[28]). In the present work, if the 229.5 keV transition were in its right position, the 152.5 keV state would be connected to the 0^-, $1^\pm$ levels by cascades of only two transitions. In that case, the most probable spin and parity values would be $I^\pi = 4^-$.

Therefore in the discusion which follows we shall use the spin and parity values $I^\pi = 5^+$, $I^\pi = 5^+$ and $I^\pi = 3^+$ respectively attributed to the 71.1, 25.7 keV levels and the ground state using the in-beam results of ref.[19]). From the decay modes of the levels established in the present decay study we can organize the level scheme as shown in fig. 7. On the left-hand side, the 3^+ and 5^+ states of the $\pi h_{9/2} \otimes \nu 1/2^-[521]$ configuration and the low-energy positive-parity levels mainly decaying to them. On the right-hand side the 5^+ state identified as the bandhead of the $\pi h_{9/2} \otimes \nu 7/2^-[514]$ configuration and the levels connected to it by the 101.5, 17.6 and 186.3 keV cascade. In the middle the 152.5 keV negative-parity state corresponding to the $\pi h_{9/2} \otimes \nu 9/2^+[624]$ configuration and the levels which could have the same configuration. The parity of the 210.8 keV level could not be determined. However, this level has been placed with the negative-parity states in the middle of fig. 7 since it decays by a low-energy transition to the 152.3 keV negative-parity level and is connected to the 320.7 keV negative-parity state.

4.3. Theoretical calculations

To go further in the understanding of the low-spin level structure in ^{182}Ir we shall now use predictions provided by coupling two quasiparticles to a rotor with variable moment of inertia, a semi-microscopic model developed by Bennour et al.[33]). The moments of inertia are deduced from the experimental energy sequence observed in the corresponding even-even core.

As a first step, to determine the static properties of the core we perform HF + BCS calculations[47-49]) using the Skyrme III force[50]) and usual pairing interaction with constant matrix elements (G_{op} = 13.5 and G_{on} = 15.2 MeV with standard cut off as suggested by dynamical calculations performed for Pt isotopes[51,52])). In this description axial symmetry is assumed, which is reasonable because the properties of the collective structures observed in the isotopes under discussion correspond to those of prolate-shaped nuclei. Furthermore, the particle number is not conserved, which means that, in principle, energy location of ^{182}Ir states can be determined from anyone of the four neighbouring even-even cores : ^{180,182}Os or ^{182,184}Pt and that states calculated for each core can belong to anyone of the four neighbouring doubly-odd nuclei. However from the occupation probabilities v^2 directly related to the location of a particle state above or under the Fermi level it is possible to guess the best core which has to be considered to represent a given configuration in ^{182}Ir. For example the v^2 values 0.94, 0.94 and 0.53 of the $1/2^-$

[521], 7/2$^-$[514] neutron and 1/2$^-$[541] (h9/2 parentage) proton states indicate that these states lie below the Fermi level in the ^{184}Pt core. Therefore the ^{184}Pt nucleus is the most convenient core to calculate the energy location for the states of the $\pi 1/2^-[541] \otimes \nu 1/2^-[521]$ and $\pi 1/2^-[541] \otimes \nu 7/2^-[514]$ configurations in ^{182}Ir . On the other hand, for the 9/2$^+$[624] neutron state which is located above the Fermi level in ^{184}Pt ($v^2 = 0.29$), we have to use the ^{182}Pt core instead.

The static equilibrium deformation of the ^{182}Pt and ^{184}Pt cores and the associated quasiparticle wave functions have been determined. Calculations have been performed within a basis including 13 oscillator shells. Since, in such a treatment, no extension of the wave function on the deformation is considered one can wonder whether the deformation of the core ground state is actually the equilibrium deformation calculated. To evaluate the sensitivity of nuclear spectroscopic properties against the core deformation we have also performed HF + BCS calculations in which the even-even core ^{184}Pt is constrained to take different deformations around the equilibrium solution.

In a second step, by means of the rotor-plus-one quasiparticle model developed by Meyer et al.[34]) we have calculated vs the deformation the energy location of the neutron states that we have afterwards compared to the observed levels in the odd-A ^{183}Pt isotope. For each deformation self consistent quasiparticle states lying at less than 5 MeV from the Fermi level have been taken into account. The spectra obtained by coupling one neutron with the ^{184} Pt core for 0.19, 0.23, 0.26 (equilibrium solution), 0.30 and 0.33 β_2 deformation parameter values are shown in fig.8 in comparison with the experimental data known for ^{183}Pt [refs.[11,12])] and ^{185}Pt [refs.[53,54])] nuclei. One can see that the 7/2$^-$[503] state is calculated at too high energy whereas the 5/2$^-$[512] is at too low energy except for $\beta_2 = 0.19$. The 9/2$^+$[624] energy has to be compared to that in ^{185}Pt since this state is located above the Fermi level. We have to note that the energy of the 7/2$^+$[633] and 1/2$^-$[521] states strikingly increases with the deformation β_2 while that of the 7/2$^-$[514] state decreases. The relative location of these states which is very sensitive to the deformation suggests that ^{183}Pt has a deformation close to $\beta_2 = 0.23$. Moreover for the proton states calculated in the same way the best agreement is also found for a β_2 value of 0.23. Furthermore, for $\beta_2 = 0.23$ there is an excellent agreement between theory and experiment for the energy location of the members of the πh9/2 structure in ^{183}Ir (fig. 9). This structure certainly plays an important role in ^{182}Ir since the h9/2 proton is present in all configurations expected to be located at low energy from the zero-order level scheme (see fig. 6).

Therefore, calculations performed for neutron states and proton states as well, indicate that the ^{184}Pt deformation is actually somewhat smaller ($\beta_2 = 0.23$) than that found for the equilibrium solution ($\beta_2 = 0.26$). It is worth noting that the binding energies for these two deformations differ by only 0.17 MeV, which corresponds to a quasi degeneracy.

We can now determine the energy location of states in ^{182}Ir using the rotor-plus-two-quasiparticle coupling model[33]). In this approach, to ensure consistency, the neutron-proton interaction is calculated using the Skyrme III force, i.e. the same force as that used to determine the properties of the core and the neutron and proton quasiparticle wave functions. Calculations have been performed with and without taking into account the proton-neutron residual interaction $V_{p\text{-}n}$, with the ^{182}Pt and ^{184}Pt cores for the equilibrium deformation[55,56]), and with the ^{184}Pt core for $\beta_2 = 0.23$. To know the influence of the $V_{p\text{-}n}$ interaction on the energy location of the states we compare the results from calculations taking into account the $V_{p\text{-}n}$ interaction with those from calculations performed without $V_{p\text{-}n}$.

Thus for the π**h9/2** $\otimes$ ν**1/2$^-$[521]** configuration , the $V_{p\text{-}n}$ interaction pushes the states with odd-spin values to lower energy relatively to the even-spin states (fig. 10). Moreover the smaller the spin value is, the stronger the effect is; for example, one can see in fig. 10 that it is around 10 keV for I = 11 and about 30 keV for I = 5 from calculations performed using the ^{184}Pt core ($\beta_2 = 0.23$). For states with spin values smaller than I = 5 the effect can be stronger but it depends on the core used in the calculations. Nevertheless, the three calculations predict the same bandhead I = 3 and the same order of low-spin states 3, 2, 5, 1, 4, 0, 7, 6 with a 0^+ state around 200 keV above the bandhead. The comparison of the band structure of the πh9/2 $\otimes$ ν1/2$^-$[521] configuration obtained using the ^{184}Pt core ($\beta_2 = 0.23$) with the experimental levels believed to correspond to this configuration suggests spin and parity assignments $I^\pi = 2^+$, 1^+ and 4^+ respectively to the 74.8, 87.4 and 95.1 keV levels shown on the left-hand side of fig. 7. The 95.1 keV level and the bandhead of the unfavoured sequence of the doubly-decoupled band recently observed in an in-beam experiment[28]) are located at almost the same energy (to within 1 keV), which suggests that they are one state only. This would confirm the spin assignment I = 4 suggested by the calculations.

As for the π**h9/2** $\otimes$ ν**7/2$^-$[514]** configuration, the interaction pushes the low-spin states with spin values smaller than I = 4 to higher energies but the effect is stronger or weaker depending on the core used. In any case the states with spin values I = 4, 5 and 6 are those located at the lowest energies in the structure, the bandhead having I = 6 and I = 4 from the calculations using the ^{182}Pt core and the ^{184}Pt core (with $\beta_2 = 0.23$ and $\beta_2 = 0.26$) respectively. The energy location of the 2^+ state is the most sensitive to the $V_{p\text{-}n}$ interaction, it is predicted at 140, 400 and 580 keV above the bandhead from the calculations performed with the ^{182}Pt core, ^{184}Pt core for $\beta_2 = 0.26$ and $\beta_2 = 0.23$. The comparison of the πh9/2 $\otimes$ ν7/2$^-$[514] band structure obtained (fig. 11) with the experimental levels that very likely belongs to this structure suggests to attribute spin and parity values $I^\pi = 4^+$, 3^+ and 2^+ to the 172.6, 190.2 and 376.5 keV levels shown on the right-hand side in fig. 7. It is worth noting that the calculations using the ^{184}Pt cores predict the 4^+ state as the bandhead, which strongly suggests to invert the 101.5 and 17.6 keV transitions. However we have to remember that the 5/2$^-$[512] neutron state is always present below

the 7/2$^-$[514] state in the theoretical predictions whereas it is about 400 keV above it in the experimental level schemes (fig. 6). The bandheads predicted for both the $\pi h9/2 \otimes \nu 7/2^-[514]$ and $\pi h9/2 \otimes \nu 5/2^-[512]$ configurations have, furthermore, the same spin value I = 4, which could lead to a strong admixture between the wave functions of these states in the theory that would not exist experimentally. This is not actually the case. Therefore the predictions concerning the energy location of the 4^+ state with respect to the 5^+ and 3^+ levels in the calculation using ^{184}Pt is not at present understood. We have to note that the 6^+ state expected at 46 keV above the 5^+ state was observed at 39 keV above the 5^+ state in the in-beam experiment[28]).

For the $\pi \mathbf{h9/2} \otimes \nu \mathbf{9/2^+[624]}$ configuration the V_{p-n} interaction slightly increases the transition energies between states from $I^\pi = 6^-$ to $I^\pi = 12^-$ and changes the energy location of states with I < 6 with respect to the $I^\pi = 6^-$ state (fig. 12) . From predictions obtained with the ^{182}Pt core, the $I^\pi = 3^-$ state in fact becomes the bandhead. In any case the $I^\pi = 6^-$ and $I^\pi = 3^-$ states are lying very close in energy and the $I^\pi = 4^-$ is expected at about 50 keV above the bandhead. The experimental results suggest that the 152.5 ± 0.3 keV level has a spin value I=4. The comparison of the calculated structure with the negative-parity levels in fig. 7 suggests that the 152.3 ± 0.3 keV level could then have a spin value I = 3. However, in this interpretation it is impossible to attribute a spin value to the 174.6 keV level. On the other hand, if the 152.5 and 152.3 keV levels were the 5^- and 3^- states respectively, the 174.6 keV level could then be the 4^- state but the agreement between experimental and theoretical results would be worse. Therefore, electron measurements are essential before going further in the interpretation. In particular, the determination of 152.4 keV transition multipolarity would undoubtedly determine the spin value of the 152.5 keV level. It is worth noting that the 152.4 keV transition is also present in the recent in-beam experiment[28]), which confirms that the 152.5 keV level observed in the present work is actually the state located at 126.9 keV in ref.[19]).

The states of the $\pi \mathbf{h9/2} \otimes \nu \mathbf{1/2^-[521]}$ and $\pi \mathbf{h9/2} \otimes \nu \mathbf{7/2^-[514]}$ configurations have been calculated using the same core. Therefore, it is possible to compare the energy distance predicted between the 3^+ ground state which is the $\pi h9/2 \otimes \nu 1/2^-[521]$ bandhead, and the 5^+ of the $\pi h9/2 \otimes \nu 7/2^-[514]$ configuration to the corresponding experimental value. The predicted 140 keV value is larger than the experimental one that is 71.1 keV. This can be related to the too large energy distance between the $1/2^-[521]$ and $7/2^-[514]$ neutron states calculated using the rotor-plus-one-quasiparticle approach with the same core (see fig. 13). At this stage, we have to remember the very large sensitivity of this energy distance versus the nuclear deformation. Furthermore, we can see in fig. 13 that the influence of the V_{p-n} interaction on the relative location of these structures is very weak (27 keV). It is worth noting that, contrary to the puzzling situation observed in the doubly-odd ^{184} Au nucleus[55-58]), the first states of these two configurations are located in the same order as the corresponding neutron state in the neighbouring

odd-A ^{183}Pt and ^{181}Os nuclei. It is shown in ref.[55]) that the inversion observed in ^{184}Au is very likely related to a deformation change effect.

We have to note that the model used in the present work was very helpful to identify the structure in the low-energy level scheme and to understand the $V_{p\text{-}n}$ influence on the different states belonging to the same structure. The predictions of the energy locations of very low-spin states remain somewhat qualitative but we have to keep in mind that such semi microscopic models are based on quite rough approximations especially for the particle-number conservation and dynamical effects (no rotation-vibration coupling).

5. COMMENT ON THE α -DECAY OF ^{186}Au

The α-ray emitted by the $I^{\pi} = 3^-$ ground state of ^{186}Au [ref.[59])] very likely feeds the 3^- state proposed at 152.3 ± 0.3 keV in ^{182}Ir since this state would have the same configuration as the ^{186}Au ground state, $\pi h9/2 \otimes \nu 9/2^+[624]$ [ref.[60])]. Therefore, the Q_α value of 4755 ± 15 keV which was reported in ref.[59]) and adopted in the latest mass evaluation[41]), should be increased by 152.3 keV. The corrected Q_α value, Q_α = 4907 ± 16 keV, is then in better agreement with the older value, Q_α = 5150 ± 380 keV, derived from systematics and given in the 1983 mass tables [61]).*

6. CONCLUSION

A low-spin level scheme of ^{182}Ir has been established, for the first time, by use of mass-separated ^{182}Au sources. Four excited states previously identified in ^{182}Ir by an in-beam experiment[19])could be observed and recognized in the present decay work, thus illustrating the complementary aspects of the two types of study. We have shown that the rotor-plus-one-quasiparticle model used in the present work is able to very well reproduce the odd-A nuclear spectra provided the core is constrained to take a deformation somewhat smaller than that of the equilibrium solution ; for the proton states of the h9/2 system the agreement is, in fact, almost perfect. Using the rotor-plus-two-quasiparticle model it has been shown that the influence of the residual $V_{p\text{-}n}$ interaction slightly depends on the core used in the calculations but is always the most important on the low-spin state energy location. However the spin sequence within one structure is almost independent of the core, which allowed us to identified some of the low-spin levels observed. Thus it has been possible to identify the 3^+, 2^+, 1^+ and 4^+ levels very likely associated to the $\pi h9/2 \otimes \nu 1/2^-[521]$ configuration, the 4^+, 3^+ and 2^+ levels corresponding to the

---

* The good agreement between the value reported by Akovali et al.[59]) and that given in the 1993 mass tables[41]) mentioned in a recent paper[62]) is only due to redundancy and therefore should not be considered.

$\pi h_{9/2} \otimes \nu 7/2^-[514]$ configuration and the 3^- state that could belong to the $\pi h_{9/2} \otimes \nu\ 9/2^+[624]$ structure. Nevertheless, electron measurements are indispensable for going further in the interpretation. Furthermore, we have shown that the V_{p-n} interaction modifies little or none the position of the various structure relatively to the zero-order level scheme provided the deformation of the doubly-odd nucleus remains similar to that of its neighouring odd-A nuclei. These results added to other ones[55-58]) strongly suggest that the inversion observed in ^{184}Au, isotone of ^{182}Ir, is due to a deformation change effect[55]).

We would like to thank the staff of the ISOCELE separator for their help during the experiment. We are indebted to the staff of the Orsay synchrocyclotron for their cooperation. We thank the Service Electronique Physique (IPN) who designed and constructed the data acquisition system and R. Breuil who continuously assisted us. We are very grateful to Prof. A.J. Kreiner, Dr. M.G. Porquet and Dr. G. Audi for fruitful discussions.

REFERENCES

1) P. Dabkiewicz et al., Phys. Lett. 82B (1979) 199
2) C. Bourgeois, P. Kilcher, B. Roussière, J. Sauvage-Letessier and M.G. Porquet, Nucl Phys. A386 (1982) 308
3) G. Ulm et al., Z. Phys. A325 (1986) 247
4) F. Hannachi et al., Z. Phys. A330 (1988) 15
5) M.G. Desthuilliers et al., Nucl. Phys. A313 (1979) 221
6) M.I. Macias-Marques et al., Nucl. Phys. A427 (1984) 205
7) J. K. P. Lee et al., 5th Int. Conf. on nuclei far from stability, Rosseau Lake, A I P Conf. Proc. 164 (1988) 205
8) K. Wallmeroth et al., Phys. Rev. Lett. 58 (1987) 1516; Nucl. Phys. A493 (1989) 224
9) G. Savard et al., Nucl. Phys. A512 (1990) 241
10) A. Visvanathan, E.F. Zganjar, J.L. Wood, R.W. Fink, L.L. Riedinger and F.E. Turner, Phys. Rev. C19 (1979) 282
11) B. Roussière, C. Bourgeois, P. Kilcher, J. Sauvage and M.G. Porquet, Nucl. Phys. A504 (1989) 511
12) J. Nyberg et al., Nucl. Phys. A511 (1990) 92
13) A. Zerrouki, Thèse 1979, Université Paris-Sud, Orsay
14) C. Schück et al., in Future Directions in Studies of Nuclei far from Stability, edited by J. H. Hamilton et al. (North-Holland, Amsterdam, 1980) p. 127
15) C. Schück, V. Berg, A. Zerrouki, J. Genevey-Rivier, A. Knipper and C. Richard-Serre, Rapport d'activité CSNSM (1978-1980) p. 21
16) U. Garg. et al., Phys. Lett. 151B (1985) 335
17) S. André et al., Phys. Rev. Lett. 38 (1987) 327
18) V.P. Janzen et al., Phys. Rev. Lett. 61 (1988) 2073
19) A.J. Kreiner, J. Davidson, M. Davidson, P. Thieberger and E. K. Warburton, Phys. Rev. C42 (1990) 878
20) J. Sauvage et al., Nucl. Phys. A540 (1992) 83
21) G.D. Dracoulis, B. Fabricius, T. Kibédi, A.P. Byrne and A.E. Stuchbery, Nucl. Phys. A554 (1993) 439
22) R. Kaczarowski, U. Garg. E.G. Funk and J.W. Mihelich, Phys. Rev. C45 (1992) 103
23) H. Kawakami et al., J. Phys. Soc. Jap. 36 (1974) 623
24) I.M. Ladenbauer-Bellis et al., Can. J. Phys. 56 (1978) 321
25) A. Neskakis et al., Nucl. Phys. A261 (1976) 189
26) C. Fahlander et al., Nucl. Phys. A375 (1982) 263
27) B. Roussière et al., Z. Phys. A351 (1995) 127
28) H. Somacal et al., to be published
29) A.J. Kreiner, D.E. Di Gregorio, A.J. Fendrik, J. Davidson and M. Davidson, Nucl. Phys. A432 (1985) 451
30) A.J. Kreiner, J. Davidson, M. Davidson, D. Abriola, C. Pomar and P. Thieberger, Phys. Rev. C36 (1987) 2309, C37 (1988) 1338E
31) J.C. Putaux et al., Nucl. Instr. Meth. 186 (1981) 321

32) P. Paris et al., Nucl. Instr. Meth. 186 (1981) 91
33) L. Bennour, J. Libert, M. Meyer and P. Quentin, Nucl. Phys. A465 (1987) 35
34) M. Meyer, J. Danière, J. Letessier and P. Quentin, Nucl. Phys. A316 (1979) 93
35) M.G. Porquet, J. Sauvage, M. Meyer and P. Quentin, Nucl. Phys. A451 (1986) 365
36) L. Bennour, Thèse 1987, Paris XI
37) S. E. P., catalogue électronique IPNO 1985
38) H. Dautet, private communication
39) R. Gummick and J. B. Niday, Computerized Analysis by γ-ray Spectrometry, UCRL 51061, Vol. 1 (1972)
40) S.E.T.I., Rapport interne IPNO 87-03
41) G. Audi and A. H. Wapstra, Nucl. Phys. A565 (1993) 1
42) N.B. Gove and M.J. Martin, Nuclear Data A10 (1971) 205
43) S. Raman and N. B. Gove, Phys. Rev. C7 (1973) 1995
44) J. Davidson et al., Z. Phys. A324 (1986) 363
45) A. Ben Braham et al., Nucl. Phys. A533 (1991) 113
46) A. Ben Braham et al., Nucl. Phys. A482 (1988) 553
47) D. Vautherin and D.M. Brink, Phys. Rev. C5 (1972) 626
48) D. Vautherin, Phys. Rev. C7 (1973) 296
49) H. Flocard, P. Quentin, A.K. Kerman and D. Vautherin, Nucl. Phys. A203 (1973) 433
50) M. Beiner, H. Flocard, Nguyen Van Giai and P. Quentin, Nucl. Phys. A238 (1975) 29
51) I. Deloncle, J. Libert, L. Bennour and P. Quentin, Phys. Lett. B233 (1989) 16
52) I. Deloncle, thèse 1989, Paris VI
53) B. Roussière, C. Bourgeois, P. Kilcher, J. Sauvage and M.G. Porquet, Nucl. Phys. A438 (1985) 93
54) B. Roussière, C. Bourgeois, P. Kilcher, J. Sauvage, M. G. Porquet and A.Wojtasiewicz, Nucl. Phys. A485 (1988) 111
55) F. Ibrahim et al., to be published
56) F. Ibrahim, thèse 1994, Paris VII
57) F. Ibrahim et al., Z. Phys. A350 (1994) 9
58) F. Ibrahim et al., NFFS6 and AMCO9 Int. Conf., Inst. Phys. Conf. Ser. n° 132 : section 5 (1992) 731
59) Y.A. Akovali et al., Phys. Rev. C42 (1990) 1130
60) M.G. Porquet, C. Bourgeois, P. Kilcher and J. Sauvage-Letessier, Nucl. Phys. A411 (1983) 65
61) A.H. Wapstra and G. Audi, Nucl. Phys. A432 (1985) 55
62) C.R. Bingham et al., Phys. Rev. C51 (1995) 125

TABLE CAPTIONS

Table 1 : γ-ray data for $^{182}Pt \rightarrow {}^{182}Ir$ decay.

Footnotes : a) $\Delta E\gamma \approx 0.2$ keV for transitions with $I\gamma > 50$ and $E\gamma < 500$ keV. $\Delta E\gamma \approx 0.3$ keV for the other transitions

b) $\Delta I\gamma \approx 15$ %.

c) Existence of the transition deduced from the coincidence relationships.

d) γ-intensity estimated from coincidence spectra.

e) γ-line mixed with a γ-ray belonging to $^{182}Ir \rightarrow {}^{182}Os$ decay.

Table 2 : Probable multipolarities and total intensity of some γ-rays belonging to the $^{182}Pt \rightarrow {}^{182}Ir$ decay.

Footnote : a) From the parity change of the initial and final states, see text.

FIGURE CAPTIONS

Figure 1 : Prompt coincident spectra for gates on the 681.5 and 656.7 keV γ-lines. Counts for the right-hand part of the spectra have been multiplied by 3 and 5 respectively.

Figure 2 : Delayed and prompt coincident spectra for gates on the 81.5 keV γ-ray. Counts for the right-hand side of the spectra have been multiplied by 6 and 3. The delayed matrix used corresponds to the left-hand side part of the time spectrum with the 81.5 keV γ-ray as a stop signal.

Figure 3 : Prompt coincident spectra for gates on the 106.8 and 286.7 keV γ-lines.

Figure 4 : Prompt coincidence spectra for gates on the 57.4 and 58.7 keV γ-rays. For the 58.7 keV gate counts for the right-hand part of the spectrum has been multiplied by 12.

Figure 5 : Partial level scheme of ^{182}Ir. The transitions which were not or too weakly observed in coincidence because of their low energy, weak intensity or their location in the level scheme are shown as dashed-lines. Levels established from coincident spectra for gate on only one γ-ray are drawn in dashed-line. The 8.1 and 172.6 keV levels are also shown in dashed-line because the order of the cascades 8.1-373.6 and 101.5-17.6 keV could not be established.

Figure 6 : Zero-order level scheme of ^{182}Ir obtained using the proton states π (on the left-hand side) and the neutron states ν (on the right-hand side) respectively observed in the odd-proton ^{181,183}Ir isotopes and the odd-neutron ^{181}Os and ^{183}Pt nuclei.

Figure 7 : Partial level scheme of ^{182}Ir, organized using the level decay modes.

Figure 8 : Theoretical neutron state spectra obtained by coupling one neutron to the ^{184}Pt core against β_2 values in comparison with the experimental data known for ^{183,185}Pt isotopes. Neutron states above the Fermi level are shown as open symbols.

Figure 9 : Theoretical proton state spectra obtained by coupling one proton to the ^{184}Pt core for β_2=0.23 in comparison with the experimental data known in ^{183}Ir (left-hand side). Comparison of the theoretical with the experimental results for the h9/2 structure (right-hand side).

Figure 10 : States of the $\pi h9/2 \otimes \nu 1/2^-[521]$ configuration calculated using the ^{184}Pt core at a deformation parameter value $\beta_2 = 0.23$ without and with taking into account the $V_{p\text{-}n}$ residual interaction.

Figure 11 : Same as fig.10 for the $\pi h9/2 \otimes \nu 7/2^-[514]$ configuration.

Figure 12 : States of the $\pi h9/2 \otimes \nu 9/2^+[624]$ configuration calculated using the ^{182}Pt core at the equilibrium solution without and with taking into account the $V_{p\text{-}n}$ residual interaction.

Figure 13 : Comparison of the energy distances observed between the $1/2^-[521]$ and the $7/2^-[514]$ neutron states in ^{183}Pt and between the first states of the $\pi h9/2 \otimes \nu 1/2^-[521]$ and $\pi h9/2 \otimes \nu 7/2^+[514]$ configurations in ^{182}Ir with those calculated using rotor-plus-one (or two)-quasiparticle approaches with the ^{184}Pt core ($\beta_2 = 0.23$).

Table 1
γ-ray data for $^{182}Pt \rightarrow {}^{182}Ir$ decay

Eγ a)	Iγ b)	Main coincident γ-rays	Location
12.6[c)]			87.4 - 74.8
17.6[c)]			(190.2 - 172.6)
22.2	~20	81, 146, 171	174.6 - 152.5
24.7	ε	146	345.5 - 320.7
44.3	8.1	75, 136	(255.1 - 210.8)
45.4	74	81, 101, 186	71.1 - 25.7
47.6	10	77	(199.9 - 152.3)
57.4	58	69, 95	152.5 - 95.1
57.7	15	136	
58.7	157	75, 77, 87	210.8 - 152.3
64.9	~7 [d)]		(152.3 - 87.4)
69.4	16	57, 246, 287	95.1 - 25.7
70.4	23	69, 287, 307, 550, 572	452.1 - 381.7
71.1	~3 [d)]		71.1 - 0
74.8	932	44, 59, 77, 110, 119, 123, 136, 184, 307, 377, 562, 792, 925	74.8 - 0
77.5	170	59, 75, 168, 681	152.3 - 74.8
81.5	370	45, 146, 171, 657, 681, 815	152.5 - 71.1
87.4	64	59, 107, 123, 172, 196, 915	87.4 - 0
95.1	5.8	57, 246, 287	95.1 - 0
97.1	3.2	X Ir	
101.5	22	45, 186, 262, 527, 572, 625, 648, 714, 813, 835	172.6 - 71.1
106.8	25	75, 87, 808	194.2 - 87.4
109.9	8.4	75, 136, 657, 681	320.7 - 210.8
111.0	~3 [d)]		452.1 - 341.2
119.5	5.2	75	194.2 - 74.8
123.4	100	75, 87, 792	210.8 - 87.4
135.9	760	44, 75, 110, 657, 679, 681, 792, 925	210.8 - 74.8
146.2	144	22, 25, 81, 152, 657, 679, 681, 704, 790, 815	320.7 - 174.6
152.4	40		152.5 - 0
156.7	2.3	458	
168.3	6.9	75, 77, 657, 681, 815	320.7 - 152.3
170.4	5.2	473	
170.9	72	22, 81, 152, 577, 657, 679, 790	345.5 - 174.6
172.0	6.1		259.3 - 87.4
184.4	46	75, 241, 339, 362, 365, 377, 387, 403, 523,594, 743, 1281	
	6		259.3 - 74.8
			636.4 - 452.1
186.3	36	101, 527, 625, 648	376.5 - 190.2
196.1	14	87, 353, 719	283.5 - 87.4
210.0	~10 [d)]	70, 262, 278, 339, 362	662.1 - 452.1
229.5	4.0	70, 572	381.7 - 152.5
241.3	5.5	75, 184, 523	
246.1	7.1	69, 95, 111, 550, 572	341.2 - 95.1
261.7	15	45, 101, 184, 210, 362, 550, 572	452.1 - 190.2
266.4	8	75, 111, 572	341.2 - 74.8
277.6	11	81, 184, 210, 362, 550, 572	452.1 - 174.6
283.4	16	353, 719	283.5 - 0
286.7	17	69, 70, 95, 184, 210, 550, 572, 620, 643	381.7 - 95.1
306.7	18	70, 75, 210, 550, 572, 620, 643	381.7 - 74.8

Table 1 - continued

Eγ a)	Iγ b)	Main coincident γ-rays	Location
339.2	7.4	70, 75, 184, 210, 403, 588	1002 - 662.1
347.6	7.4	70	
352.6	3.9		636.4 - 283.5
361.7	18	70, 75, 184, 210, 262, 403, 588	1024.3 - 662.1
365.0	21	75, 87, 184, 353, 377, 549, 562	1002 - 636.4
373.6	6.0	70, 572	(381.7 - 8.1)
376.8	27	75, 87, 172, 184, 365, 387	636.4 - 259.3
381.6	2.9	70	(381.7 - 0)
387.5	10 d)	75, 87, 184, 377, 549, 562	1024.3 - 636.4
	7 d)	157, 458, 615	
390.8	6.0	87	
402.7	10	75, 184, 339, 362	662.1 - 259.3
425.4	5.7	77	
457.9	11	157, 388	
472.5	16	75, 77	
473.6	11	97	
520.2	8.0	X Ir	
523.2	13	75, 184, 241	
527.0	8.0	101, 186	903.9 - 376.5
549.3	5 d)	87, 365, 387	636.4 - 87.4
549.6	17 d)	70, 262, 278, 287, 307	1002 - 452.1
561.8	30	75, 365, 387	636.4 - 74.8
572.2	36	45, 70, 101, 262, 287, 307	1024.3 - 452.1
576.9	~6 d)	146, 171	
588 c)	~6 d)	75, 339, 362	662.1 - 74.8
593.6	9.3	75, 184	852.9 - 259.3
615.1	5.3	387	
620.4	7.8	287, 307	1002 - 381.7
625.3	14	101, 186	1002 - 376.5
642.7	8.1	287, 307	1024.3 - 381.7
647.8	13	101, 186	1024.3 - 376.5
656.7	99	22, 81, 146, 171	1002 - 345.5
679.3	21	81, 146, 171	1024.3 - 345.5
681.5	180	22, 81, 110, 146, 168	1002 - 320.7
684.2	6.4	X Ir	
704.1	23	81, 146	1024.3 - 320.7
714	3 d)		903.9 - 190.2
718.9	6.7	87, 196, 283	1002 - 283.5
743.3	3.9	184	1002 - 259.3
790.3 e)	~34 d)	81, 146, 171	1135.8 - 345.5
791.7	31	59, 75, 87, 123, 136	1002 - 210.8
808.2	4.6	87, 107	1002 - 194.2
812.4	9	101	1002 - 190.2
815.1	51	81, 110, 146	1135.8 - 320.7
827.1	12	X Ir	852.9 - 25.7
834.8	8.3	101	1024.3 - 190.2
915.2	12	87	1002 - 87.4
925.1	6.4	75, 136	1135.8 - 210.8
1281	~6 d)	75, 184	1540 - 259.3

Table 2

Probable multipolarities and total intensity of some γ-rays in $^{182}Pt \rightarrow {}^{182}Ir$ decay

Eγ (keV)	Level intensity balance Level		Coincident Intensity Gate		Probable multipolarities	I_{tot}
12.6						150
22.2	152.5	not E2			E1, M1	120 << 2000
24.7						80 << 130
45.4	71.1	not E1	186	not E2	M1	920
57.4	95.1	not E2, M2			E1 [a]	80
58.7	152.3	not E2			E1, M1	210 << 1000
69.4	95.1	not E1			not E1	≥ 70
70.4	381.7	not E2			E1, M1	30 << 100
74.8	74.8	not E1	59 107 123	M1	M1	3400
77.5			59 107 123	E1	E1	300
81.5	71.1	E1			E1	620
101.5	172.6	not E1			not E1	≥ 120
146.2	320.7	not E1			not E1	≥ 300

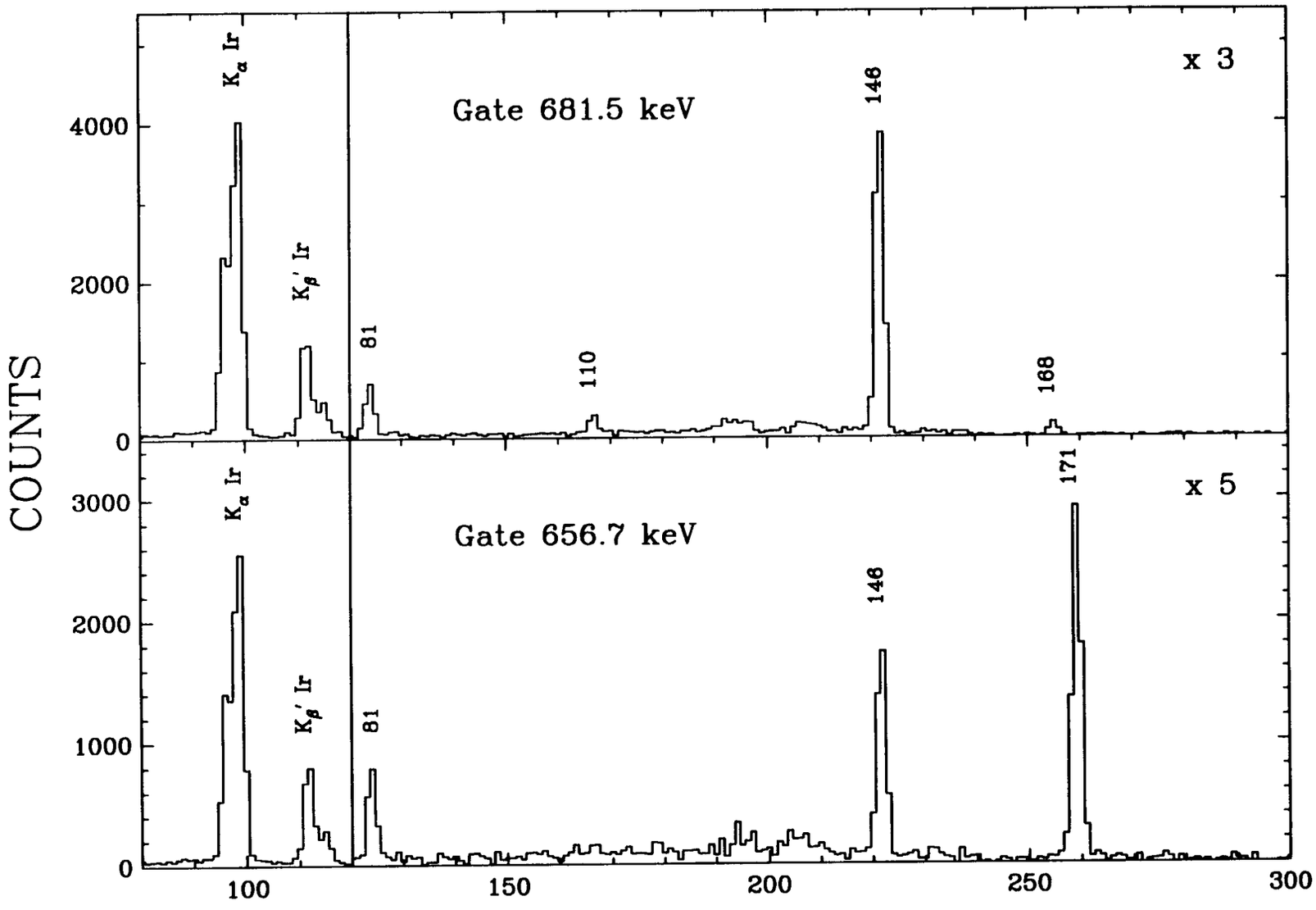
Gate 681.5 keV
x 3
Gate 656.7 keV
x 5
K_α Ir
K_β' Ir
81
110
146
168
171
COUNTS
CHANNEL NUMBER
0
1000
2000
3000
4000
100
150
200
250
300

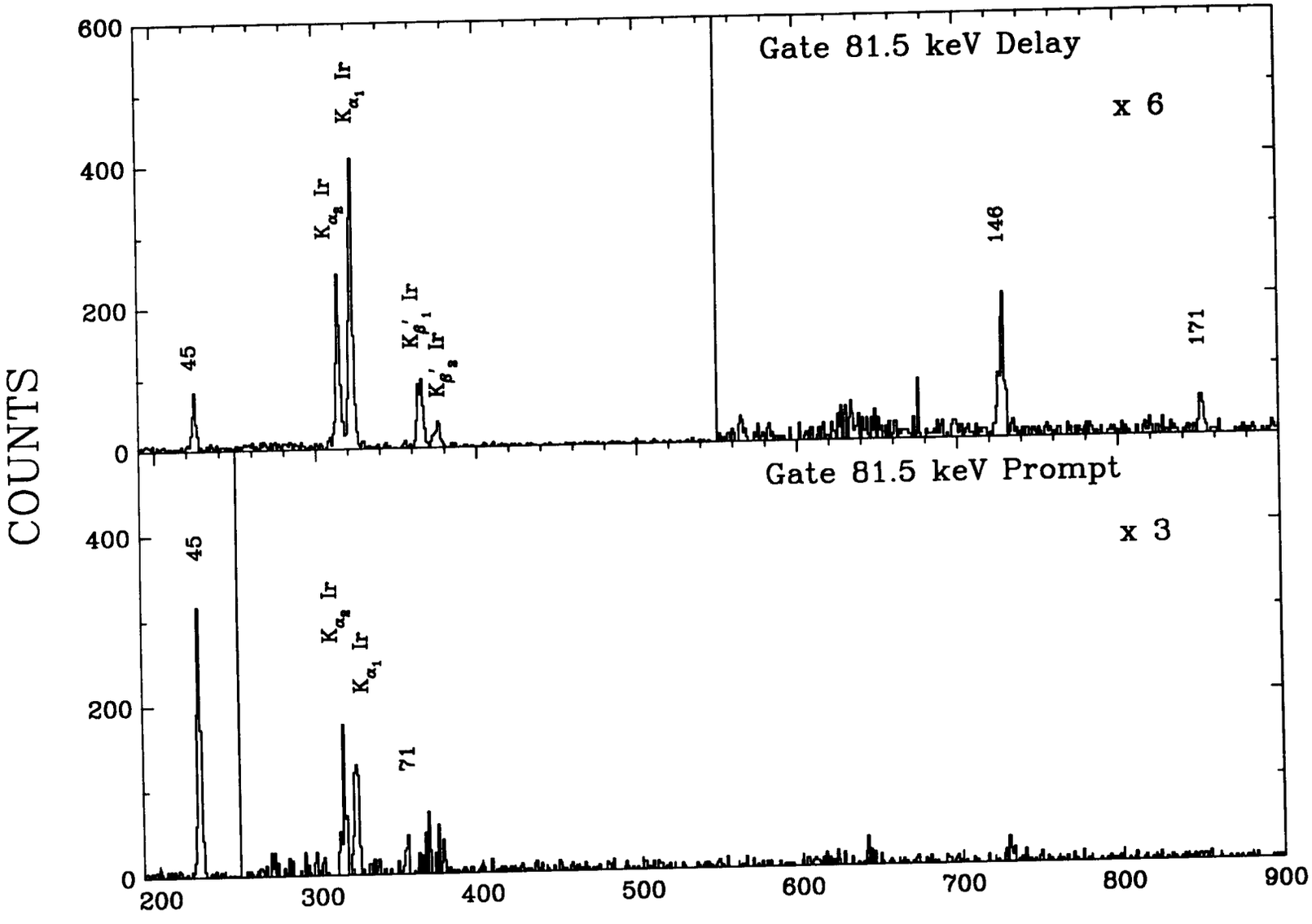
Gate 81.5 keV Delay
x 6
Gate 81.5 keV Prompt
x 3
COUNTS
CHANNEL NUMBER
45
146
171
71
K_{α_1} Ir
K_{α_2} Ir
K'_{β_1} Ir
K'_{β_2} Ir
0
200
400
600
200
300
400
500
600
700
800
900

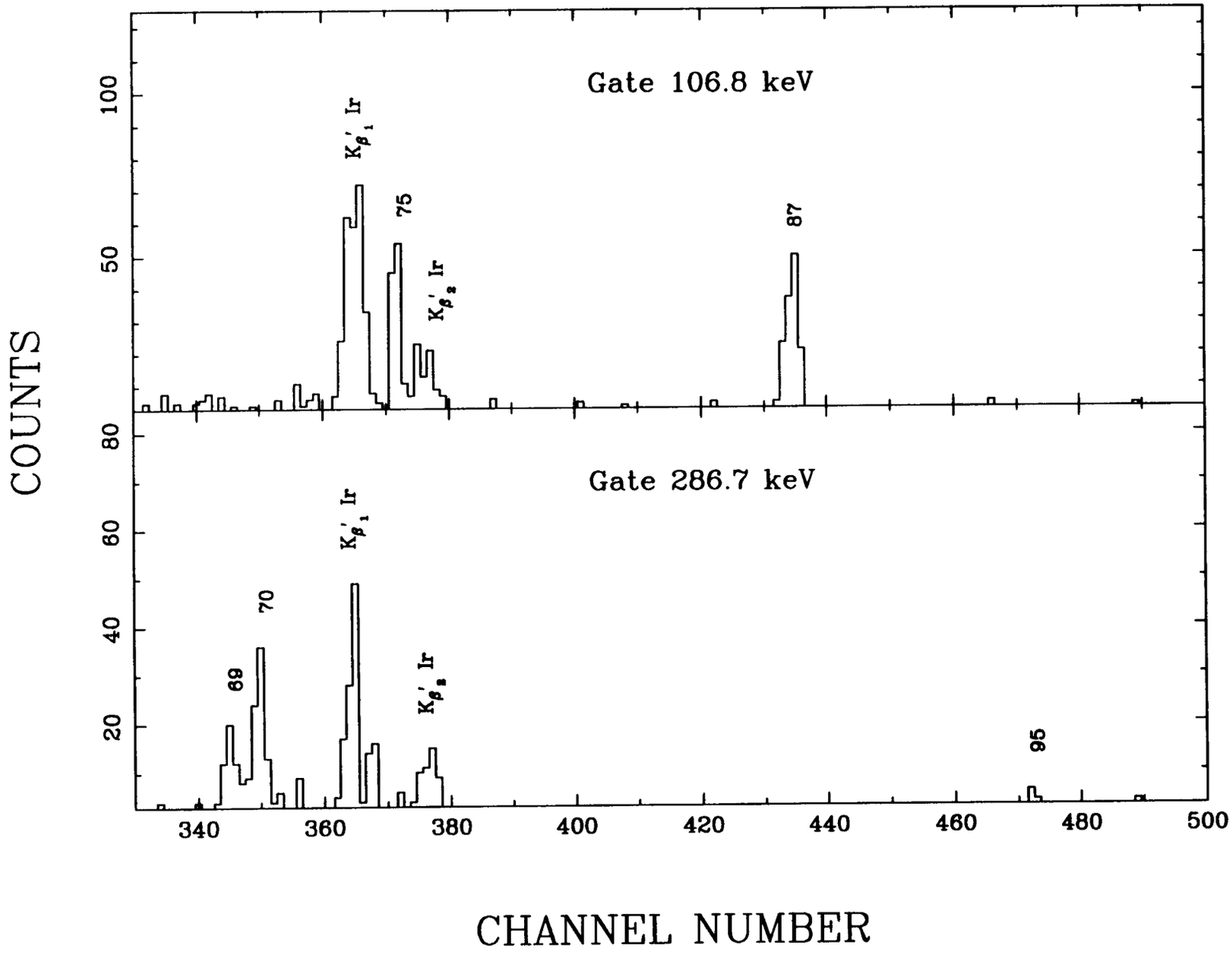
Gate 106.8 keV
Gate 286.7 keV
COUNTS
CHANNEL NUMBER
$K_{\beta_1'}$ Ir
$K_{\beta_2'}$ Ir
75
87
69
70
95
100
50
80
60
40
20
340
360
380
400
420
440
460
480
500

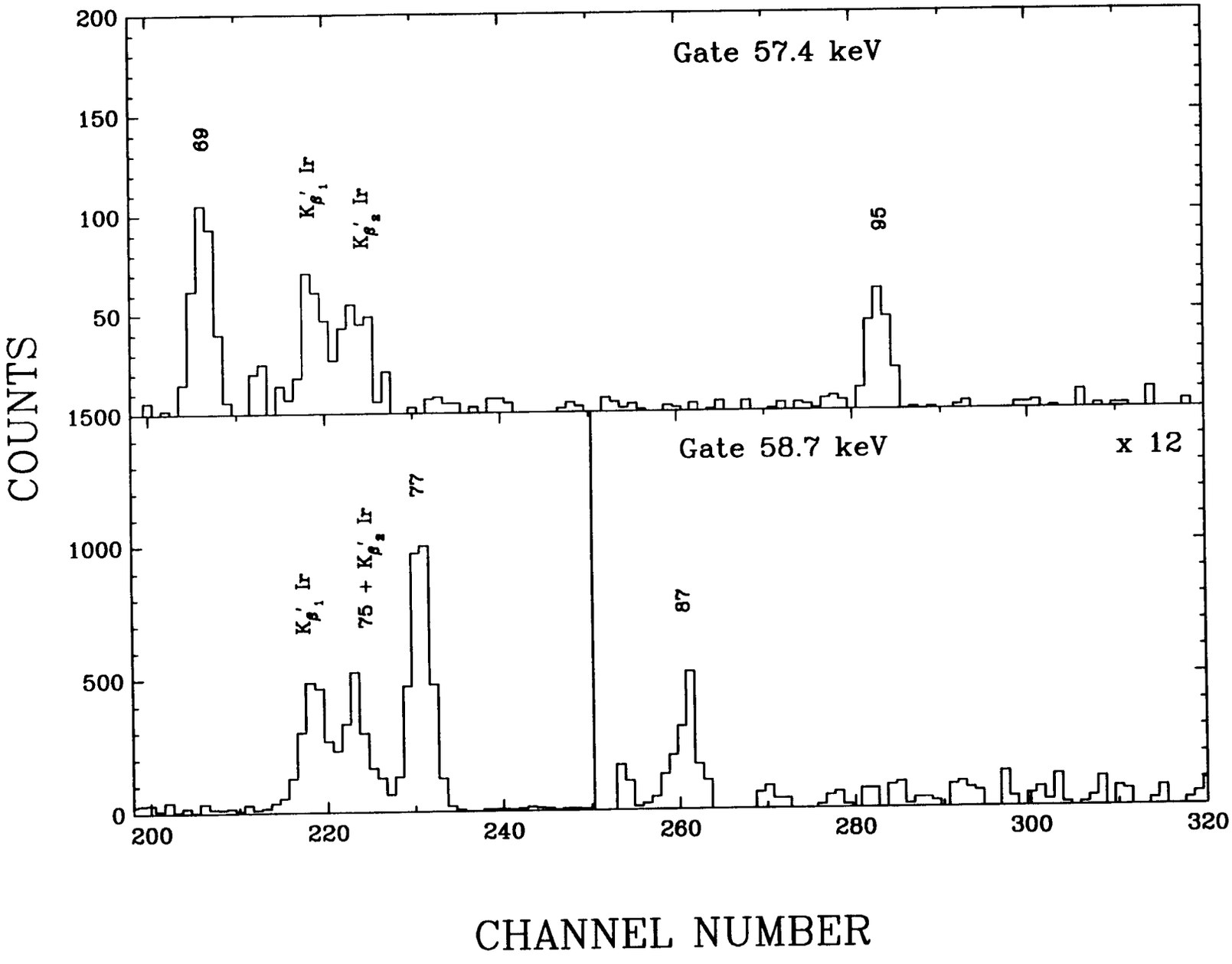
Gate 57.4 keV
69
$K_{\beta_1'}$ Ir
$K_{\beta_2'}$ Ir
95
Gate 58.7 keV
x 12
$K_{\beta_1'}$ Ir
75 + $K_{\beta_2'}$ Ir
77
87
COUNTS
CHANNEL NUMBER
200
150
100
50
1500
1000
500
0
200
220
240
260
280
300
320

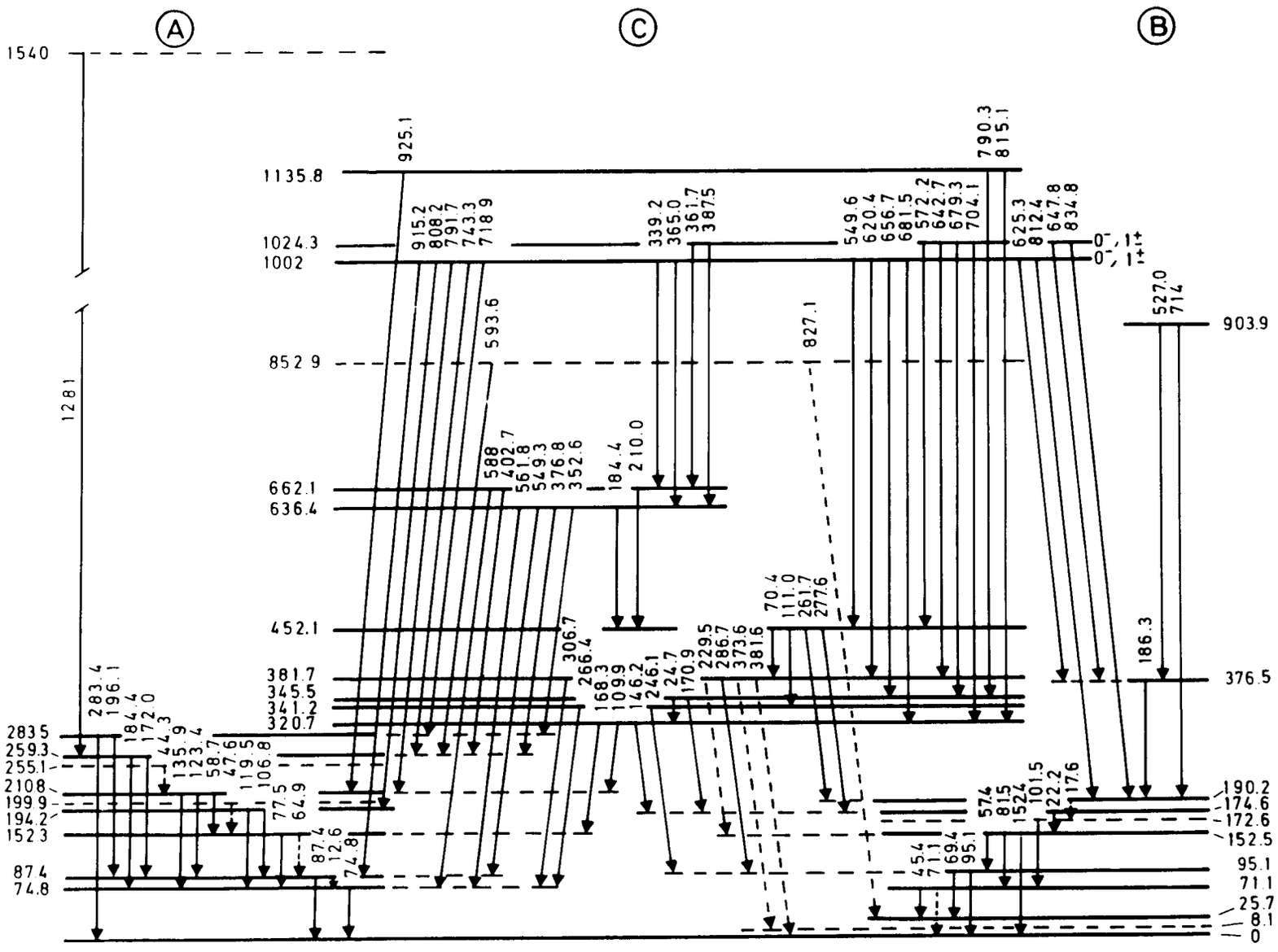
A
C
B
1540
1281
1135.8
1024.3
1002
852.9
662.1
636.4
452.1
381.7
345.5
341.2
320.7
283.5
259.3
255.1
210.8
199.9
194.2
152.3
87.4
74.8
925.1
915.2
808.2
791.7
743.3
718.9
593.6
588
402.7
561.8
549.3
376.8
352.6
339.2
365.0
361.7
387.5
184.4
210.0
827.1
790.3
815.1
549.6
620.4
656.7
681.5
572.2
642.7
679.3
704.1
625.3
812.4
647.8
834.8
0⁻, 1⁺
0⁻, 1⁺
527.0
714
903.9
186.3
376.5
70.4
111.0
261.7
277.6
306.7
266.4
168.3
109.9
146.2
246.1
24.7
170.9
229.5
286.7
373.6
381.6
283.4
196.1
184.4
172.0
44.3
135.9
123.4
58.7
47.6
119.5
106.8
77.5
64.9
87.4
12.6
74.8
574
815
1524
101.5
22.2
117.6
454
71.1
69.4
95.1
190.2
174.6
172.6
152.5
95.1
71.1
25.7
8.1
0

fig. 5

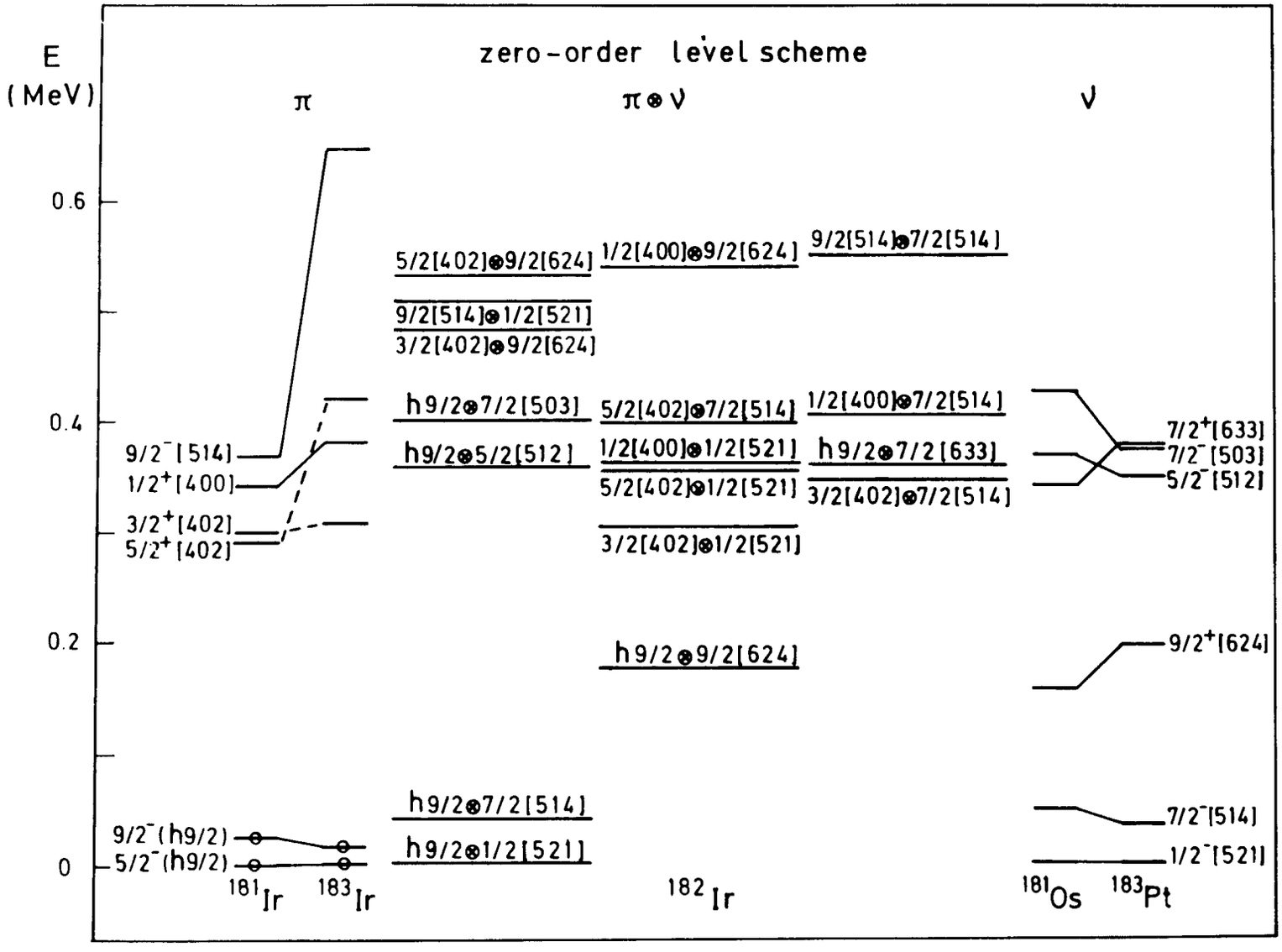
zero-order level scheme
E
(MeV)
π
π⊗ν
ν
0.6
0.4
0.2
0
9/2⁻[514]
1/2⁺[400]
3/2⁺[402]
5/2⁺[402]
9/2⁻(h9/2)
5/2⁻(h9/2)
181Ir
183Ir
5/2[402]⊗9/2[624]
9/2[514]⊗1/2[521]
3/2[402]⊗9/2[624]
h9/2⊗7/2[503]
h9/2⊗5/2[512]
h9/2⊗7/2[514]
h9/2⊗1/2[521]
1/2[400]⊗9/2[624]
5/2[402]⊗7/2[514]
1/2[400]⊗1/2[521]
5/2[402]⊗1/2[521]
3/2[402]⊗1/2[521]
h9/2⊗9/2[624]
182Ir
9/2[514]⊗7/2[514]
1/2[400]⊗7/2[514]
h9/2⊗7/2[633]
3/2[402]⊗7/2[514]
7/2⁺[633]
7/2⁻[503]
5/2⁻[512]
9/2⁺[624]
7/2⁻[514]
1/2⁻[521]
181Os
183Pt

fig. 6

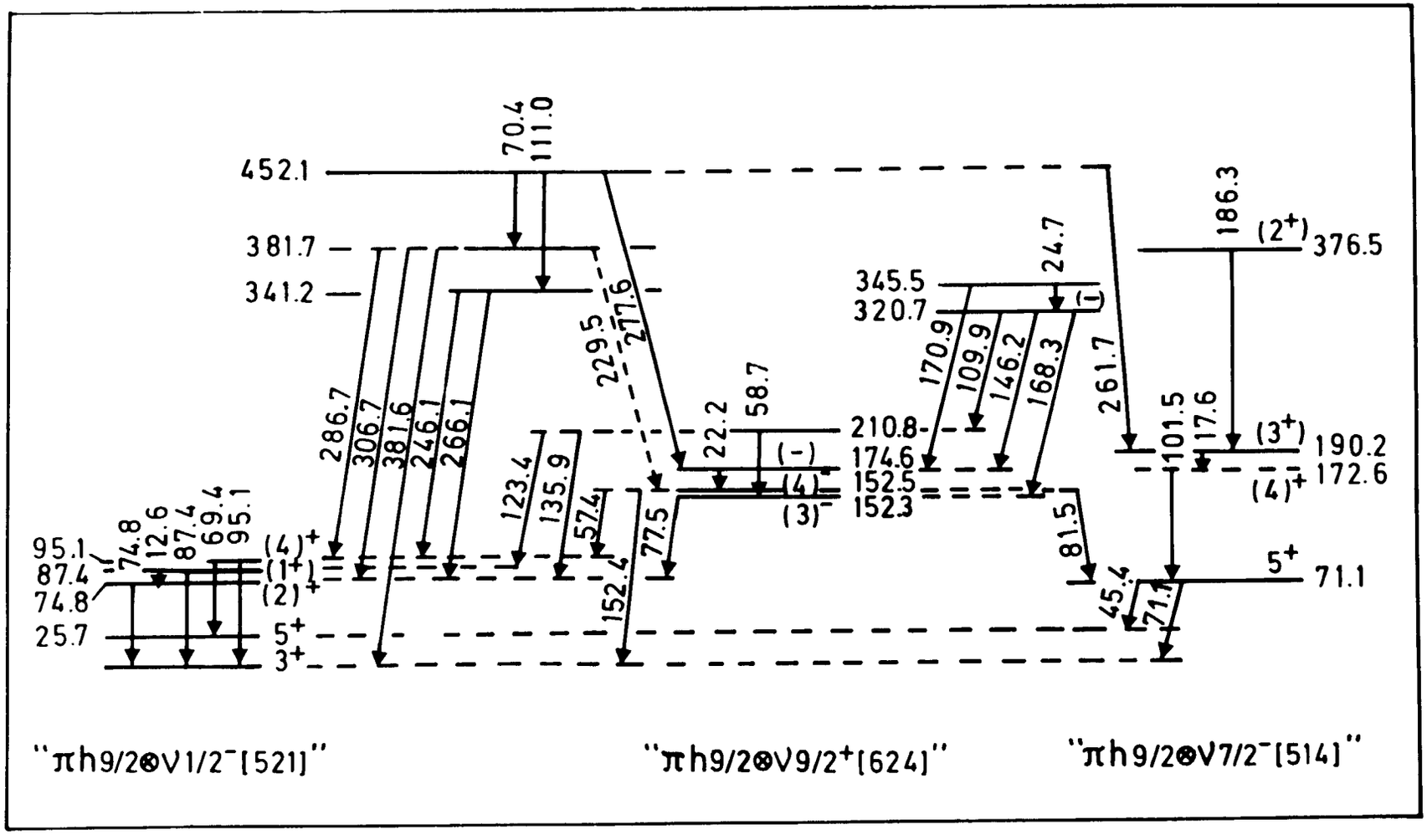
452.1
381.7
341.2
70.4
111.0
286.7
306.7
381.6
246.1
266.1
229.5
277.6
22.2
58.7
210.8
174.6
152.5
152.3
(-)
(4)
(3)
123.4
135.9
57.4
77.5
152.4
95.1
87.4
74.8
25.7
(4)+
(1+)
(2)+
5+
3+
74.8
12.6
87.4
69.4
95.1
345.5
320.7
24.7
(1)
170.9
109.9
146.2
168.3
261.7
186.3
(2+) 376.5
101.5
17.6
(3+) 190.2
(4)+ 172.6
81.5
45.4
71.1
5+ 71.1
"πh9/2⊗ν1/2⁻[521]"
"πh9/2⊗ν9/2⁺[624]"
"πh9/2⊗ν7/2⁻[514]"

fig. 7

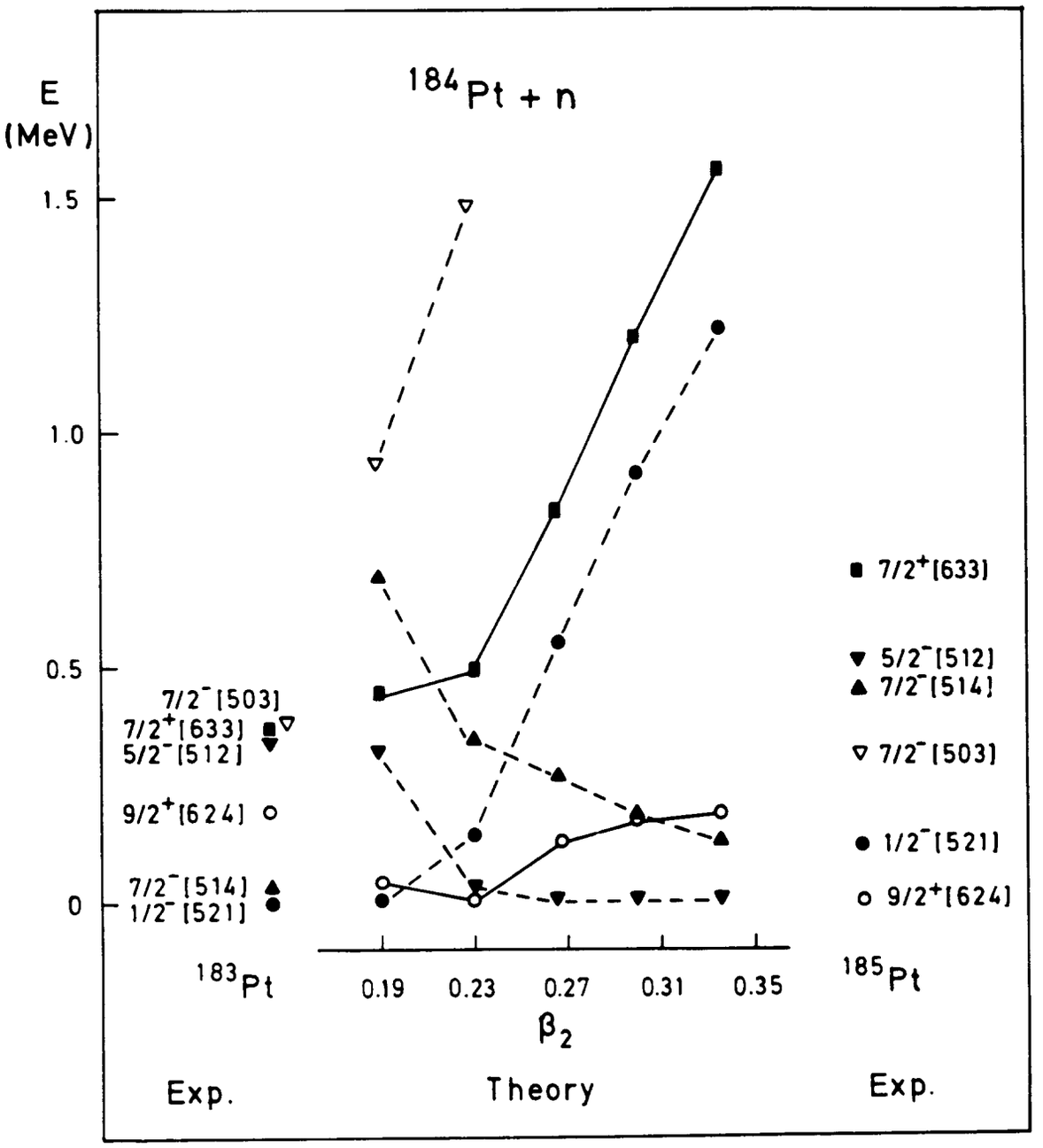
E
(MeV)
1.5
1.0
0.5
0
184Pt + n
7/2⁻[503]
7/2⁺[633]
5/2⁻[512]
9/2⁺[624]
7/2⁻[514]
1/2⁻[521]
183Pt
Exp.
0.19
0.23
0.27
0.31
0.35
β2
Theory
7/2⁺[633]
5/2⁻[512]
7/2⁻[514]
7/2⁻[503]
1/2⁻[521]
9/2⁺[624]
185Pt
Exp.

fig. 8

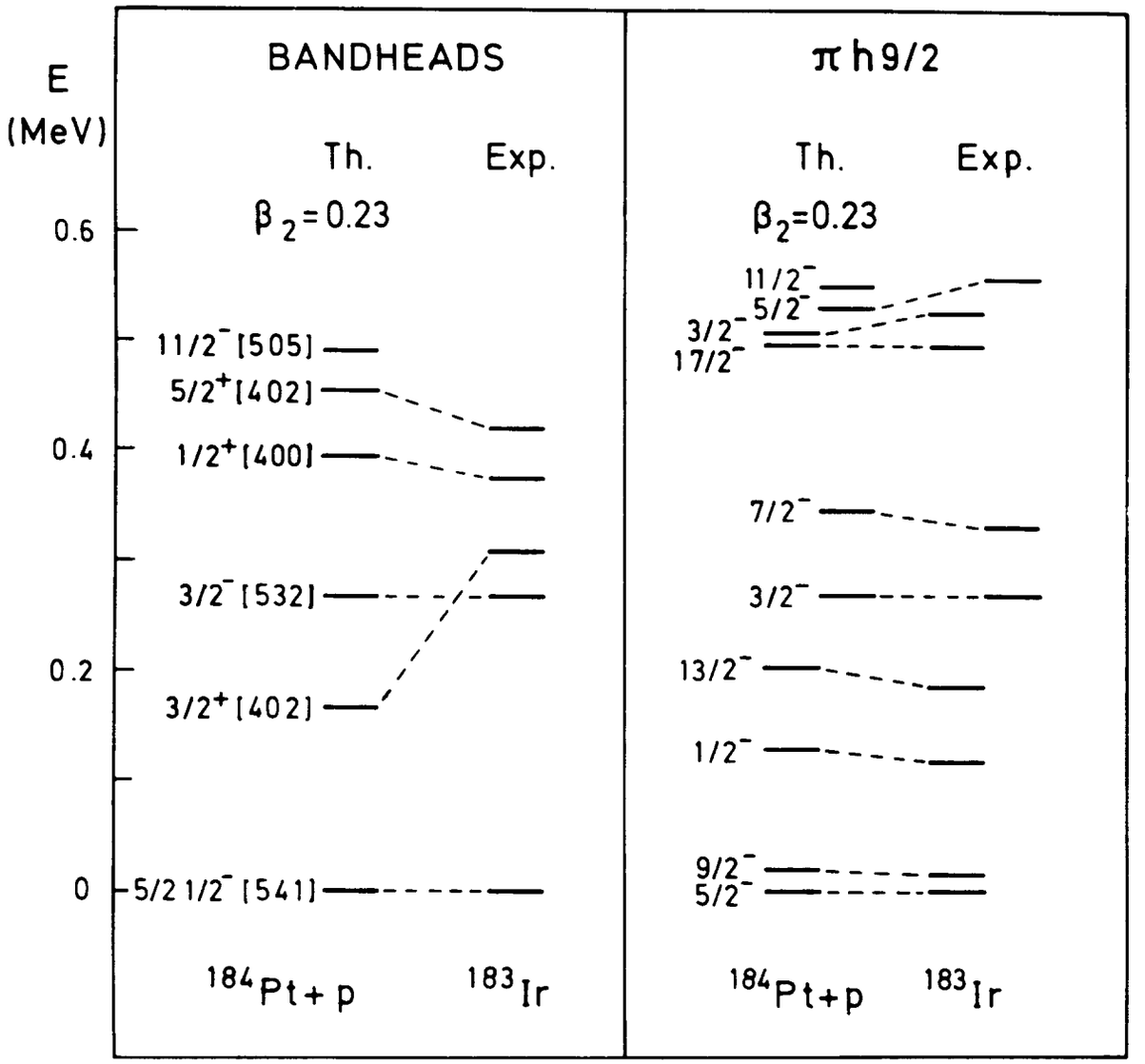
E
(MeV)
BANDHEADS
Th.
Exp.
β2=0.23
0.6
0.4
0.2
0
11/2⁻[505]
5/2⁺[402]
1/2⁺[400]
3/2⁻[532]
3/2⁺[402]
5/2 1/2⁻[541]
184Pt+p
183Ir
πh9/2
Th.
Exp.
β2=0.23
11/2⁻
5/2⁻
3/2⁻
17/2⁻
7/2⁻
3/2⁻
13/2⁻
1/2⁻
9/2⁻
5/2⁻
184Pt+p
183Ir

fig. 9

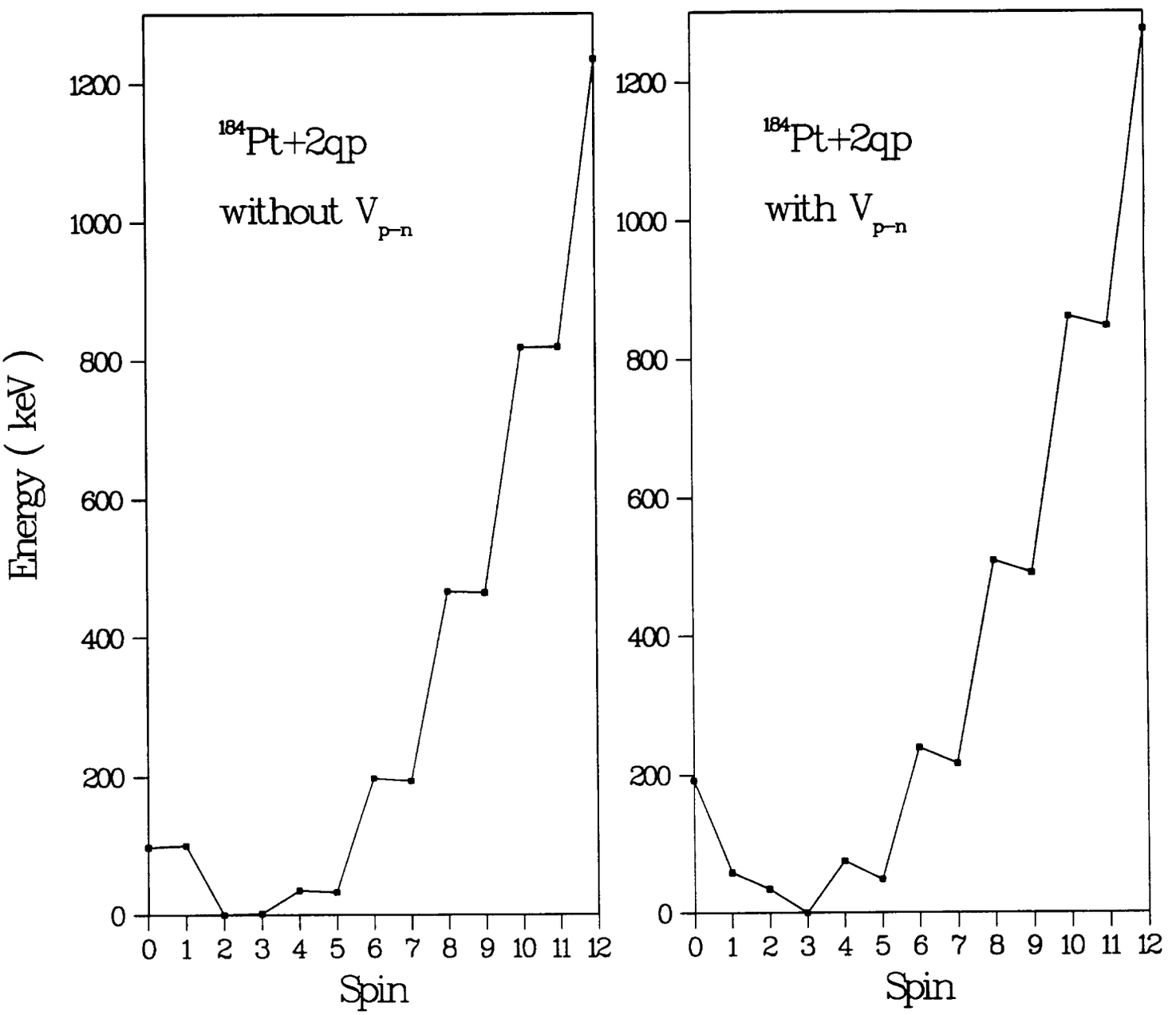
Energy (keV)
1200
1000
800
600
400
200
0
^{184}Pt+2qp
without V_{p-n}
0 1 2 3 4 5 6 7 8 9 10 11 12
Spin
^{184}Pt+2qp
with V_{p-n}
0 1 2 3 4 5 6 7 8 9 10 11 12
Spin

Fig. 20

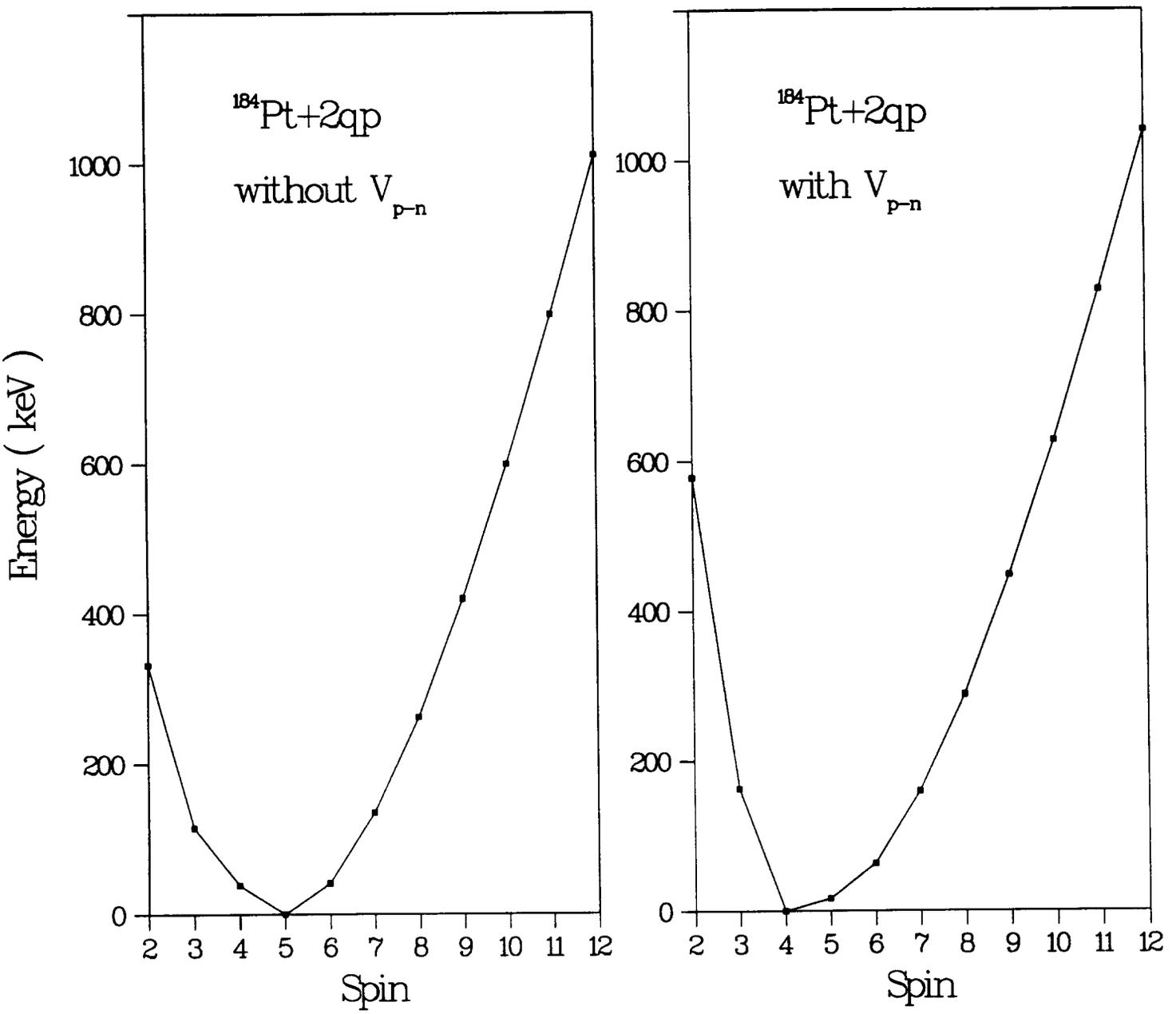
^{184}Pt+2qp
without V_{p-n}
^{184}Pt+2qp
with V_{p-n}
Energy (keV)
0
200
400
600
800
1000
2 3 4 5 6 7 8 9 10 11 12
Spin
Spin

Fig. 11

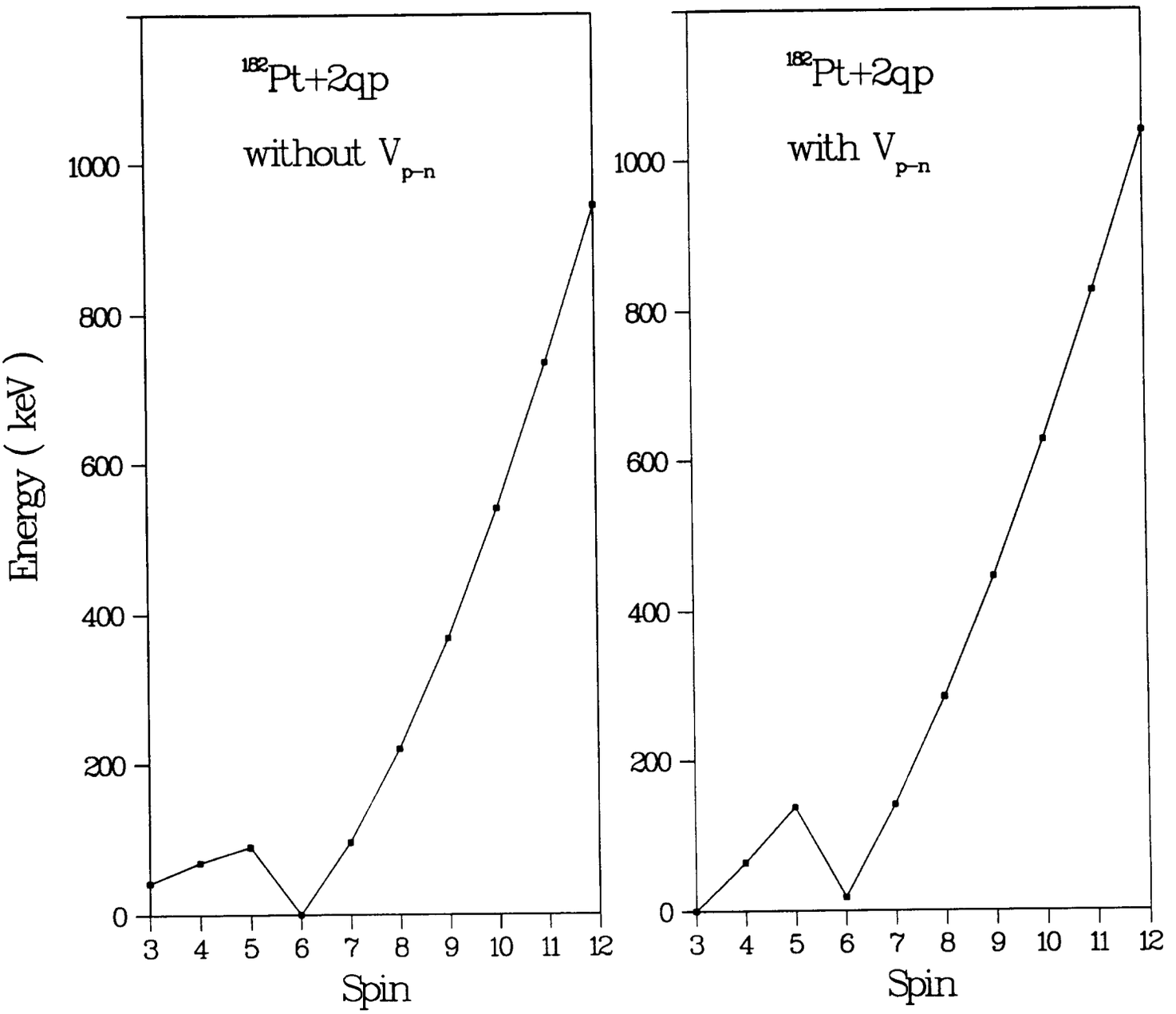
^{182}Pt+2qp
without V_{p-n}
^{182}Pt+2qp
with V_{p-n}
Energy (keV)
0
200
400
600
800
1000
3
4
5
6
7
8
9
10
11
12
Spin
Spin

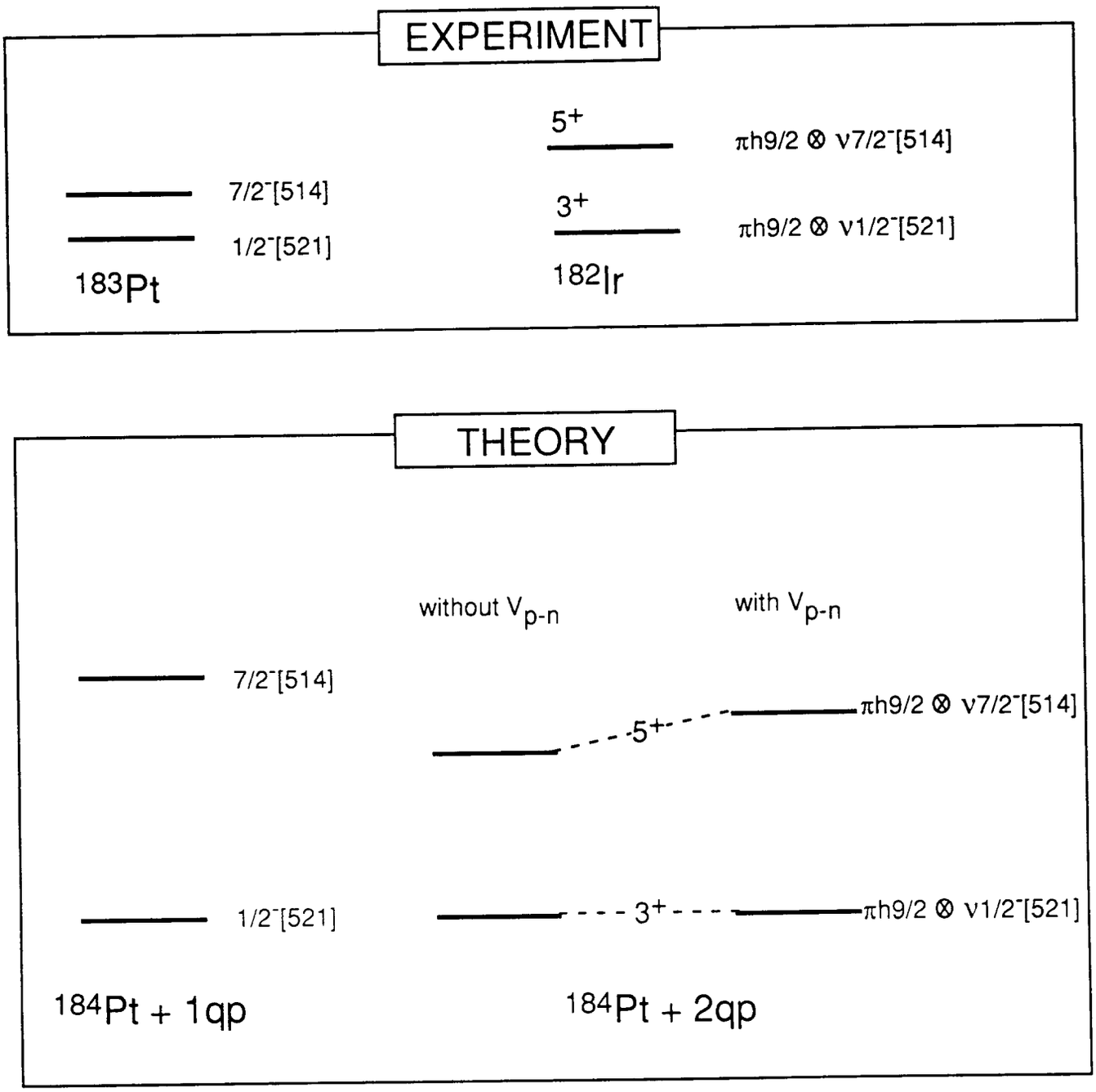
EXPERIMENT
5+
πh9/2 ⊗ ν7/2-[514]
3+
πh9/2 ⊗ ν1/2-[521]
7/2-[514]
1/2-[521]
183Pt
182Ir
THEORY
without Vp-n
with Vp-n
7/2-[514]
πh9/2 ⊗ ν7/2-[514]
5+
1/2-[521]
3+
πh9/2 ⊗ ν1/2-[521]
184Pt + 1qp
184Pt + 2qp